Co-option of *Plasmodium falciparum* PP1 for egress from host erythrocytes

Aditya S. Paul[1], Alexandra Miliu[2], Joao A. Paulo[3], Jonathan M. Goldberg[1], Arianna M. Bonilla[1],

Laurence Berry[2], Marie Séveno[2], Catherine Braun-Breton[2], Aziz L. Kosber[1], Brendan Elsworth[1],

Jose S.N. Arriola[1], Maryse Lebrun[2], Steven P. Gygi[3], Mauld H. Lamarque[2], Manoj T.

Duraisingh[1]

[1]Department of Immunology and Infectious Diseases, Harvard T. H. Chan School of Public

Health, Boston, USA, 02115.

[2]Laboratory of Pathogen Host Interaction (LPHI), Centre National de la Recherche Scientifique

(CNRS), Université de Montpellier, Montpellier, France.

[3]Department of Cell Biology, Harvard Medical School, Boston, USA, 02115.

Abstract

Asexual proliferation of the *Plasmodium* parasites that cause malaria follow a developmental program that alternates non-canonical intraerythrocytic replication with dissemination to new host cells. We carried out a functional analysis of the *Plasmodium falciparum* homolog of Protein Phosphatase 1 (*Pf*PP1), a universally conserved cell cycle factor in eukaryotes, to investigate regulation of parasite proliferation. *Pf*PP1 is indeed required for efficient replication, but is absolutely essential for egress of parasites from host red blood cells. A phosphoproteomic screen and chemical-genetic analysis provided evidence for a HECT E3 protein-ubiquitin ligase, as well as a fusion protein with guanylyl cyclase and phospholipid transporter domains, as functional targets of *Pf*PP1. Extracellular phosphatidylcholine stimulates *Pf*PP1-dependent egress. Parasite *Pf*PP1 acts as a master regulator that can integrate multiple cell-intrinsic pathways with external signals to direct parasite egress from host cells.

Main Text

Malaria parasites from the genus *Plasmodium* follow an unusual developmental program during infection of erythrocyte host cells, utilizing a non-canonical style of asexual proliferation, known as schizogony, to undergo multiple cycles of nuclear replication before a single cytokinesis event (*1-3*). Merozoites, the mature parasite forms, must infect new host cells to initiate new intraerythrocytic developmental cycles (IDC) and sustain proliferation, achieved only through egress from the host cell for release into circulation. Protein phosphorylation in parasites is developmentally regulated in blood-stage growth (*4*), and genetic studies show that roughly one-half of the *Plasmodium* protein kinase and protein phosphatase genes are essential for the IDC (*5-16*). Protein Phosphatase 1 (PP1) is a highly conserved and ubiquitous enzyme in eukaryotes that regulates mitotic exit and cytokinesis (*17-21*). With functions also in non-cell cycle-related processes [reviewed in (*22*)], PP1 is a dominant contributor to total cellular phosphatase activity (*23-26*). For the *Plasmodium falciparum* homolog of PP1 (*Pf*PP1*)* (*27*), genetic evidence for likely essentiality (*6, 8, 28*), high levels of expression compared to other protein phosphatase genes (*29, 30*) (fig. S1A), and the identification of several binding proteins (*31-39*), suggest multiple roles in blood-stage parasites.

To investigate *Pf*PP1-mediated regulation of the IDC and parasite proliferation, we initiated a reverse genetic analysis. With a transgenic *P. falciparum* line expressing a triple-hemagglutinin (HA$_3$) tag at the 3'-end of the endogenous *pfpp1* gene (fig. S1B,C), we found that *Pf*PP1 protein is expressed throughout the 48-hr IDC, becoming upregulated from approximately the midpoint until the end (Fig. 1A). In accord with recent reports for PP1 in the rodent malaria parasite *Plasmodium berghei* (*35*), we observed nuclear and cytoplasmic localization of the enzyme, with cytoplasmic *Pf*PP1 becoming predominant as the parasite matures (fig. S1D). Cell cycle stage-

dependent compartmentalization of PP1 has been reported in lower eukaryotes, consistent with distinct functions for the enzyme (*40*). To assess the function of *Pf*PP1 in blood-stage proliferation, we generated a transgenic line of *P. falciparum* for inducible knockout of the *pfpp1* gene (*pfpp1*-iKO), based on the dimerizable Cre recombinase (DiCre) system (fig. S1E-G) (*41*, *42*). Induction of *pfpp1*-knockout by rapamycin treatment early in the IDC, ~3-5 hrs post-invasion (hpi), results in strong reduction of *Pf*PP1 protein levels by ~30 hpi (Fig. 1B; fig. S1B,G). By following DNA replication through the IDC, we found that early-iKO of *pfpp1* delays parasite development before resulting in the accumulation of multinucleate schizont forms, blocked prior to egress (Fig. 1C). Reverse genetic analysis by inducible expression thus establishes the essentiality of *Pf*PP1 for asexual proliferation.

To investigate *Pf*PP1-function at specific times through the IDC, we used a transgenic *P. falciparum* line for conditional knockdown (fig. S2A-C). Knockdown of *Pf*PP1 fused to a Destabilization Domain (DD)-tag, induced through depletion in culture of the DD-stabilizing small molecule Shield-1 (Shld1) (*11*, *43*, *44*), confirms essentiality of the enzyme to blood-stage parasites (Fig. 1D,E; fig. S2D,E). We confirmed late IDC-stage expression of the enzyme and cytoplasmic localization in mature parasites (fig. S2F,G). To map the time of function of *Pf*PP1, we induced knockdown at different stages of the IDC and measured DNA replication. We measured phenotypes with knockdown induced at the immature ring stage preceding the growth phase (4 hpi), at trophozoites before the onset of DNA replication (24 hpi), and early in schizogony (33 hpi) (Fig. 1F). With destabilization of *Pf*PP1-DD in rings, we observed significant defects in DNA replication (Fig. 1F; fig. S2H). Knockdown induced in trophozoites or early schizonts permits DNA replication (Fig. 1F; fig. S2I) but results in parasites with reduced numbers of nuclear centers (Fig. 1G; fig. S2J), suggesting defects in nuclear division.

73   Electron microscopy of *Pf*PP1-DD knockdown parasites indicate failure to complete the terminal

74   mitosis and cytokinesis step of the IDC (fig. S2K), suggesting cell cycle-regulatory functions for

75   *Pf*PP1 conserved from non-parasitic eukaryotes (*19-21*). Defects upstream of cytokinesis with

76   *Pf*PP1-DD knockdown are supported by immunofluorescence analysis; we observe that the inner

77   membrane complex (IMC, antigen *Pf*GAP45) that separates replicated, intracellular parasites

78   fails to form (fig. S2L).

79   To map functions for *Pf*PP1 late in the IDC, we induced knockdown in schizonts (~44 hpi),

80   revealing an acute requirement of the phosphatase for egress after complete DNA replication and

81   nuclear segregation (Fig. 1H,I). Knockdown elicits a complete block in host cell egress and

82   erythrocyte re-invasion (Fig. 1H; fig. S2M,N). Partial knockdown late in the IDC elicits

83   sublethal defects in egress without additional defects observed in the further transition to invaded

84   erythrocytes (egress-to-invasion) (Fig. 1J), suggesting a specific and primary function in late

85   stage schizonts.

86   The effects of late *Pf*PP1-DD knockdown are recapitulated in the *pfpp1-iKO* line with induction

87   of Rapa-mediated iKO later in the IDC (30 hpi, fig. S3A), resulting in depletion of *Pf*PP1 protein

88   at the late schizont stage (Fig. 2A). Late iKO blocks passage to new erythrocytes without defects

89   in DNA replication or nuclear segregation (Fig. 2B,C; fig. S3B). Electron microscopy shows that

90   parasites having undergone late *pfpp1*-iKO display gross morphology typical of maturation,

91   including intact erythrocyte membranes, parasitophorous vacuoles that completely house

92   parasites within, and individual parasite cells physically distinguished by plasma membranes

93   indicating the completion of cytokinesis (Fig. 2D). Immunofluorescence microscopy to image

94   markers for the parasite plasma membrane (antigen *Pf*MSP1) and the underlying IMC (antigen

95   *Pf*MTIP1) confirm cytokinesis and segregation of these structures into replicated parasites (Fig.

2E,F). Immunofluorescence shows also that secretory organelles utilized for invasion, micronemes (antigen *Pf*AMA1) and rhoptry necks (antigen *Pf*RON4), form normally with iKO of *pfpp1* (Fig. 2E,F). In the *Pf*PP1-DD line, immunofluorescence shows that parasites induced for knockdown late in the IDC undergo cytokinesis (IMC antigen *Pf*GAP45) and form normal rhoptries (antigen *Pf*RhopH3) (fig. S3E,F).

To initiate egress from erythrocytes at the close of the IDC, parasites secrete the protease *Pf*SUB1 in a regulated fashion from exoneme organelles into the lumen of the parasitophorous vacuole and activate a proteolytic cascade for sequential rupture of the vacuolar (PVM) and host cell membranes (*45-47*) (Fig. 2G). To permit assessment of PVM rupture, we endogenously tagged the PVM protein *Pf*EXP2 at the C-terminus with GFP (*48*) in the *pfpp1-iKO* background (fig. S3H-J). Late in the IDC, *Pf*EXP2-GFP in intact PVMs presents intraerythrocytically as a circular label around the parasites or between replicated parasites, while disintegration of the PVM can be observed by the appearance of fluorescent membrane fragments in parasites treated with E64 to prevent host cell rupture (Fig. 2H) (*48*). We used labeling by *Pf*EXP2-GFP to test the requirement for *Pf*PP1 in PVM rupture, finding that late induction of iKO blocks the process in virtually all parasites examined (Fig. 2H). We further used immunofluorescence analysis to assess *Pf*SUB1 release required to initiate PVM rupture (*47*), finding that rapamycin-treated *pfpp1-iKO* parasites fail to secrete the protease from exonemes (Fig. 2I). We observed that discharge of micronemes is also blocked by *pfpp1*-iKO (Fig. 2J). Our findings indicate an essential function for *Pf*PP1 at an early step of egress, following merozoite formation but upstream of discharge of the specialized parasite organelles carrying proteases and other factors utilized for rupture of surrounding membranes.

Our reverse genetic analysis establishing the function of *Pf*PP1 at egress places a factor typically associated with the conventional cell cycle of eukaryotes at a post-replicative stage of the IDC, specifically required for parasitism and spread of infection. To test if dephosphorylation of protein substrates accounts for the requirement for *Pf*PP1 in parasites late in the IDC, we implemented a chemical-genetic approach (*49*) to measure functional interaction between *Pf*PP1 and calyculin A, an active-site inhibitor of eukaryotic PP1 (*50*, *51*) (Fig. 3A). We found that knockdown significantly increases the sensitivity of egress-to-invasion by parasites to calyculin A but not to the control antimalarial drug dihydroartemisinin (DHA) (Fig. 3B), supporting a role for *Pf*PP1 phosphatase activity for function. To identify potential substrates of *Pf*PP1 and probe regulation of parasites in the late IDC, we carried out a global phosphoproteomic analysis of *Pf*PP1-DD function spanning a period in the IDC from post-replication through egress, collecting samples from highly synchronized (+/-45 min) *Pf*PP1-DD-intact and knockdown parasites at 48-hpi (4 hrs induction), and at 55-hpi (11 hrs induction) (Fig. 3C). We identified a total of 4720 phosphorylation sites from 1170 phosphoproteins, indicating phosphorylation of ~1/3 of all *P. falciparum* proteins detected in late-stage parasites (Fig. 3D; Tables S1-S3). We detected a comparable or greater number of phosphorylation sites than totals reported in other phosphoproteomic studies of late-stage *P. falciparum* (*12*, *52-55*). Our dataset thus provides a comprehensive view of phosphorylation events with tight time-resolution through the course of egress. At the earliest timepoint following induction of *Pf*PP1-DD knockdown in late in the IDC, there are minimal changes in either the global proteome or phosphoproteome between Shld1-supplemented and knockdown samples, indicating the absence of widespread global changes that may complicate assessment of specific phosphatase functions (Fig. 3D; see Supplementary Text related to figs. S4A-C).

141 *P. falciparum* homologs of established PP1 regulators for cell cycle progression (*18, 19, 56-59*),

142 the nuclear protein sds22 [in parasites, termed LRR1 for leucine-rich repeat protein 1 (*39*)] and

143 inhibitor-2 (I2) (*38*), are among the two most strongly increased factors in protein expression

144 upon *Pf*PP1-knockdown (Fig. 3D). Perturbed expression of these regulators may indicate a

145 conserved function mediated by parasite *Pf*PP1, while an increase in factors for glycolysis and

146 the pentose phosphate pathway suggest association with the proliferative state of parasites (Table

147 S4) (*60*). At 48 hpi, we observe by both phosphoproteomics and separately by immunoblot

148 analysis increased phosphorylation (by up to ~5-fold) of Ser-29 of *Pf*histone H3 (Fig. 3D; fig.

149 S4D), homologous to Ser-28 in the human ortholog studied as a phosphorylation site targeted by

150 PP1 during mitotic exit and interphase (*61, 62*). We thus observe among both putative regulators

151 and substrates evidence for conserved PP1 activity in *P. falciparum*.

152 The 50 proteins increased >2-fold in phosphorylation upon *Pf*PP1-DD knockdown (Fig. 3D,

153 Table S3) include chromatin factors (histone H3 variant, histone deacetylase 1, chromodomain-

154 binding protein), transcription factors from the AP2 family, and vacuolar-protein-sorting family

155 proteins (VPS11 and VPS18). To focus on potential substrates for essential *Pf*PP1 function at

156 egress, we identified gene products that specifically increase in transcriptional expression late in

157 the IDC (Fig. 3D). The top hit from our phosphoproteomic screen, based on magnitude of change

158 in phosphorylation with *Pf*PP1-knockdown, is a previously uncharacterized, late IDC-stage

159 protein carrying a ~300-amino acid HECT E3 protein-ubiquitin ligase domain at the C-terminus

160 (PF3D7_0628100) (Fig. 3D,E; fig. S4E). In addition to the highly upregulated phosphorylation

161 site (Ser-6138), knockdown of *Pf*PP1-DD also reveals a strongly downregulated site (>4-fold,

162 Tyr-9244); the protein also contains a previously predicted site for interaction with *Pf*PP1 (*34*)

163 near the HECT domain (Fig. 3E; fig. S4E). At >10,000 amino acids, the protein is the largest in

164 the *P. falciparum* proteome (Fig. 3E; fig. S4E).

165 The large protein, which we name here *Pf*HECT1, is the one HECT domain-containing gene of 4

166 total in *P. falciparum* to become increased in expression late in the IDC (fig. S4E). To test for

167 specific HECT activity in parasites late in the IDC, we tested for susceptibility to the small

168 molecule heclin (Fig. 3F). Heclin was identified as a broad-spectrum inhibitor of mammalian

169 HECT enzymes, with biophysical studies suggesting that direct binding by the compound

170 interferes with conformational changes necessary to catalyze transfer of ubiquitin from the E2

171 adaptor protein to an active-site cysteine in the E3 ligase (*63*). In *Pf*PP1-DD parasites stabilized

172 with Shld1, we established the anti-malarial activity of heclin toward parasites, with short (~4

173 hrs) and longer periods of exposure (~24 hrs) preceding egress exhibiting similar potency toward

174 establishment of ring-stage parasites (IC50 ~20 μM), indicating major inhibitory activity in

175 schizonts (Fig. 3F). While *Pf*PP1-DD destabilization does not increase DNA replication defects

176 induced by heclin (fig. S4F), knockdown in parasites late in the IDC strongly increases

177 susceptibility of egress-to-invasion to the inhibitor, reducing the IC50 by >100-fold to

178 submicromolar levels (Fig. 3G; fig. S4G). An assessment of schizont rupture confirms specific

179 inhibition by heclin toward egress, with dependence on *Pf*PP1 (fig. S4H). Phosphoproteomic

180 analysis (Fig. 3D) with chemical-genetic analysis (Fig. 3G) indicates a critical role for *Pf*PP1 in

181 activation of *Pf*HECT1-mediated E3 protein-ubiquitin ligase activity.

182 Among other late IDC-stage *P. falciparum* genes showing increased phosphorylation with

183 *Pf*PP1-knockdown is a guanylyl cyclase (GC) domain-containing protein encoded by the gene

184 PF3D7_0381400 (Fig. 3D, 4A), required for production of cyclic guanosine monophosphate

185 (cGMP) to stimulate the downstream effector *Pf*Protein Kinase G (*Pf*PKG) and egress from

186   infected erythrocytes (*9*, *47*, *64*). Termed GCα, the protein is present across apicomplexan

187   parasites, and in *Toxoplasma gondii* is also essential for egress (*65-68*). Given the function we

188   identified for *Pf*PP1 in egress, we implemented chemical-genetics to test for functional

189   interaction with components of cGMP-mediated signal transduction. To artificially raise cellular

190   cGMP in parasites late in the IDC, we used zaprinast, a cGMP-specific phosphodiesterase (PDE)

191   inhibitor (*47*, *69*, *70*) (Fig. 4A). The susceptibility of egress-to-invasion by *Pf*PP1-DD parasites

192   to zaprinast becomes sharply increased with knockdown: IC50 values drop by as much as ~400-

193   fold to submicromolar levels (Fig. 4A; fig. S5B). Functional interaction of *Pf*PP1 with the

194   *Pf*PKG inhibitor Compound-1 (Cpd1) (*9*), by contrast, is weak, with measurements of egress-to-

195   invasion showing no chemical-genetic interaction (Fig. 4A). An assessment of egress shows

196   increased sensitivity to Cpd1 with *Pf*PP1-DD knockdown, though much less than the level of

197   functional interaction observed with zaprinast (Fig. S5C). Our analysis of parasites late in the

198   IDC indicates a primary function for *Pf*PP1 in suppression of guanylyl cyclase activity,

199   restricting cGMP-mediated activation of *Pf*PKG upstream of numerous egress and invasion

200   processes (*54*, *71*). We note that in parental, genetically unmodified parasites, Shld1 does not

201   affect sensitivity to calyculin A, heclin, or zaprinast (fig. S5D), indicating that the chemical-

202   genetic interactions we have observed here with *Pf*PP1-DD knockdown result from impairment

203   of phosphatase function.

204   The protein GCα implicated by our analysis is fused at its N-terminus to a putative P4-ATPase

205   phospholipid transporter (PLT) domain predicted to translocate phospholipids from the

206   exoplasmic to the cytoplasmic face of membranes. The fusion of PLT with the GC domain is a

207   structure found only in alveolates (*72*), and we observed that *Pf*PP1-responsive phosphorylation

208   sites (1.4-2.6-fold upregulation with knockdown) cluster in a parasite-specific cytoplasmic loop

209   of PLT containing a catalytic site predicted essential for P4-ATPase activity (Fig. 4A; fig. S5A).

210   Mutational analysis in *T. gondii* GCα indicates the requirement for fusion of the PLT and GC

211   domains as well as ATP-dependent catalysis by the PLT (*65*, *66*), raising the possibility of a role

212   for phospholipids in proper function of the protein, perhaps in egress. To directly assess

213   involvement of phospholipids in *Pf*PP1-regulated egress, we administered synthetic

214   phospholipids to parasites late in the IDC. We tested phosphatidic acid (PtdA), known to

215   stimulate host cell egress in *T. gondii* when added extracellularly (*65*) and also through

216   endogenously synthesized forms resulting from intracellular phosphorylation of the neutral lipid

217   diacylglycerol (DAG) (*73*, *74*). We also tested phosphatidylcholine (PtdC), the major species of

218   phospholipid in host serum at concentrations of ~1-2 mM (*75*, *76*). In parasites with intact

219   *Pf*PP1-DD (300 nM Shld1), neither phospholipid influences egress (fig. S5E). In parasites with

220   partially destabilized *Pf*PP1-DD, however, PtdA and PtdC stimulate egress by up to ~1.5 and ~3-

221   fold, respectively, with effects observed at as low as 5 µM phospholipid (Fig. 4B). An effect for

222   PtdA might be explained by the proposal that the molecule provides one of multiple signals

223   required for efficient egress, acting on targets to activate microneme secretion and parasite

224   motility, downstream of cGMP and phosphatidylinositol signaling (*71*, *74*, *77*). We indeed

225   observed that knockdown of *Pf*PP1-DD late in the IDC increases susceptibility to the DAG-

226   kinase inhibitor R59022 that restricts endogenous PtdA synthesis (fig. S5F), consistent with a

227   pro-egress function for the phospholipid in *Plasmodium* parasites (*73*).

228   A role for PtdC in egress, has not been described. We found that extracellular DAG stimulates

229   egress to similar levels at similar doses as PtdC, suggesting convergent targets or efficient

230   conversion between the two lipids upon incorporation into the parasite from the extracellular

231   medium (Fig. 4B). In contrast, lysophosphatidylcholine (LPC), which drives parasite PtdC

232   biosynthesis via the Kennedy Pathway (*78, 79*), stimulates egress weakly in comparison to direct

233   administration of the phospholipid (Fig. 4B); and glucose supplementation to increase

234   endogenous DAG (*78, 80*) does not stimulate egress (Fig. S5G).

235   While erythrocyte membranes housing developing *P. falciparum* parasites block access to free

236   PtdC (*78*), host cells abruptly become permeable to extracellular solutes in the seconds to

237   minutes preceding egress (*46, 48, 81*), presenting a route for direct interaction between parasites

238   and circulating phospholipids. We thus tested accessibility of parasites to PtdC during egress,

239   using a fluorescent analog (labeled with TopFluor, TF). In most conditions we observed that TF-

240   PtdC marks only the outer membranes of erythrocytes housing multinucleate schizonts (Fig. 4C).

241   We observed clear labeling of parasites within infected erythrocytes, however, only at a later

242   timepoint when parasites have naturally entered the egress program and acquired host cell

243   permeability (Fig. 4C). The intact schizont with permeable erythrocyte membrane is a transient

244   state prior to egress, stabilized by E64-treatment (*46, 81-83*). We conclude that circulating PtdC

245   accesses parasites when host cells become permeable to the extracellular environment, shortly

246   before natural host cell rupture.

247   Endogenous PtdC is promoted with the addition of the precursor choline (*78, 79*). We found that

248   choline stimulates egress in parasites with partially destabilized *Pf*PP1-DD; albeit in contrast to

249   PtdC, only at non-physiological serum levels (*84*) (Fig. 4D). Identical, high concentrations of

250   choline do not influence egress by parasites with intact *Pf*PP1-DD (300 nM Shld1) (fig. S5H).

251   We found that high choline decreases susceptibility of parasites specifically to heclin and

252   zaprinast (Fig. 4E). Our analysis suggests that the extrinsic PtdC signal for egress interacts with

253   cell-intrinsic pathways regulated by *Pf*PP1.

254   We have functionally characterized *Pf*PP1 through the blood-stage IDC of malaria parasites. In

255   addition to potential conserved roles in development, *Pf*PP1 is absolutely essential for egress. At

256   the pre-erythrocytic liver-stage, analysis by other researchers shows the non-essentiality of PP1

257   for intrahepatocytic development, though a function for the phosphatase in egress into the

258   bloodstream was not assessed (*28*). *Pf*PP1 regulates egress of parasites through multiple

259   pathways including *Pf*HECT1 (fig. S6). Chemical inhibition by heclin (*63*) suggests a role for

260   ubiquitination alongside well-established pathways for phosphorylation and proteolysis. At

261   multiple stages of the *Plasmodium* lifecycle, signaling by cGMP is utilized for colonization of

262   new host niches, and studies indicate that a specific timing of activation and level of the second

263   messenger are critical for infectivity (*47, 85-87*). The use of *Pf*PP1 at the blood-stage to suppress

264   cGMP upstream of *Pf*PKG and *Pf*SUB1 may suggest an interface between the parasite

265   maturation and egress programs (Fig. 4F; fig. S6). We additionally discovered extracellular PtdC

266   as an extrinsic serum factor to stimulate egress from erythrocytes, distinct from the extracellular

267   LPC signal that suppresses differentiation to sexual-stage forms at an earlier point in the IDC

268   (*78*). We propose that *P. falciparum* uses PLT-GCα to translocate PtdC from the serum across

269   the parasite plasma membrane to provide a late signal to stimulate egress (Fig. 4F; fig. S6). Our

270   study demonstrates that the *Plasmodium* homolog of PP1 is a regulatory nexus for egress from

271   erythrocytes, balancing cell-intrinsic pathways with environmental signals to ensure release of

272   invasive parasites into circulation and infection of new host cells.

273

274

275

276

Methods

Reagents and antibodies

Rapamycin (LC laboratories), E64 (Sigma-Aldrich, Cat. No E3132); dihydroartemisinin (Sigma-Aldrich, Cat. No. D7439), calyculin A (Sigma-Aldrich, Cat. No. C5552), heclin (Sigma-Aldrich, Cat. No. SML1396), zaprinast (MP Biomedicals, Cat. No. ICN15693180), were each prepared in DMSO. Choline chloride (Sigma-Aldrich, Cat. No. 7527) was prepared in water. DAG and all phospholipids with mono-unsaturated diacylglycerol backbone (16:0, 18:1) from Avanti [PtdA, Cat. No. 840857; PtdC, Cat. No. 850457; TopFluor-PtdC, Cat. No. 810281; and DAG, Cat. No. 800815] were solubilized at 1 or 5 mM in 100% methanol, except PtdC (water: ethanol: methanol; 1:1:2). LPC (Cat. No. 855675) was solubilized at 200 mM in a 1:1 mixture of ethanol and water. Compound-1 (DMSO-based) was a gift from Dr. Jeffrey Dvorin (Boston Children's Hospital). Dilutions and sources for antibodies for immunoblot or immunofluorescence analysis are as follows: rabbit anti-GAP45 (1:5000, gift from Dr. Julian Rayner, Wellcome Trust Sanger Institute, Hinxton, UK); mouse anti- RhopH3 (1:200, gift from Jean-Francois Dubremetz); rabbit α-MTIP (1:500, gift from Tony Holder, The Francis Crick Institute, UK), mouse α-MSP1.19 (1:1000, gift from M. Blackman, The Francis Crick Institute, UK), mouse α-RON4 [1:200, home-made (89)], mouse α-SUB1 (1:2, gift from M. Blackman), rabbit α-AMA1 (1:1000, gift from M. Blackman); rabbit anti-histone H3 (1:10,000, Abcam); rat anti-HA antibody 3F10 (1:1000, Roche); rabbit anti-*Pf*aldolase-HRP (Abcam, 1:2000) , mouse anti-GFP (Roche, 1:1000). Shield-1 (Shld1) was synthesized as described (43, 90, 91) and dissolved to 1 mM stock concentration in absolute ethanol before use.

Plasmids

299   Primers for PCR amplification and verification of transgenesis in *P. falciparum* are shown in

300   Table S5. Transgenic parasites *pfpp1*-HA$_3$ were obtained using the plasmid pLN-PP1-HA$_3$-loxP.

301   To generate the plasmid pLN-PP1-HA$_3$-loxP , we first introduced between the BamHI and HpaI

302   sites in pLN-ENR-GFP (*92*) a synthetic fragment with sequence for a triple hemagglutinin tag

303   (HA$_3$) followed by a stop codon and a loxP site (IDT DNA), and multiple cloning sites upstream

304   of the tag. The resulting plasmid pLN-PP1-HA$_3$-loxP was further modified to target endogenous

305   *pfpp1* with HA$_3$ and loxP by introduction of a 5' homology region for the gene (HR1, 682 bp of

306   genomic DNA sequence for exons 2 and 3) fused to a recodonized synthetic fragment (IDT

307   DNA) for exons 4 and 5. The PCR-amplified elements were ligated in a single reaction step by

308   In-Fusion cloning (Clontech) upstream of the HA$_3$ tag in XmaI and AfeI sites of pLN-HA$_3$-loxP.

309   The *pfpp1* 3' homology region (HR2) carrying 440 bp of the *pfpp1* 3'-UTR was PCR-amplified

310   and inserted by In-Fusion reaction 3' of the loxP site between PstI and HpaI. The guide RNA

311   sequence for targeting *pfpp1* near exon 3 was cloned into the BbsI sites in pDC2-cam-co-Cas9-

312   U62-hDHFR (gift from M. Lee). For subsequent engineering of a *pfpp1* conditional knockout in

313   parasites, the pLN-PP1-loxPint plasmid was modified with introduction of the following

314   elements ligated in 5' to 3' order between the BamHI and ApaI sites of pLN-ENR-GFP: PCR-

315   amplified fragment of *pfpp1* encompassing 5'UTR and part of exon 1 (382 bp), a synthetic

316   fragment for a recodonized 3' sequence of exon 1 followed by the artificial loxPint (IDT DNA),

317   and a PCR-amplified fragment of the 5' end of *pfpp1* exon 2 (601 bp). The plasmid for the guide

318   RNA targeting *pfpp1* near exon 1 was constructed as above. To endogenously tag *Pf*EXP2 with

319   GFP, we generated plasmid pLN-*Pf*EXP2-GFP as described (*48*). Two homology regions for the

320   gene *pfexp2* were cloned in pLN-ENR-GFP on both sides of the GFP coding sequence: 549 bp of

321   *pfexp2* 3' coding sequence without the stop codon in frame with GFP, and 453 bp of *pfexp2*

15

322 3'UTR downstream of GFP. The *pfexp2* guide RNA sequence (*48*) was cloned into the BbsI sites

323 of pDC2-cam-co-Cas9-U62-hDHFR. Plasmid pAK8 for 3'-single crossover HA-DD-tagging at

324 endogenous *pfpp1* was constructed in the pJDD41 background (*11*) with the PCR-amplified

325 genomic insert ligated between the NotI and XhoI restriction sites. All plasmid sequences were

326 verified before downstream applications.

327 <u>Parasite culture, transfection, and synchronization</u>

328 D10 or 3D7 (Walter and Eliza Hall Institute), or p230p-based parasites (*41*) were cultured

329 continuously in human erythrocytes (*93*) obtained from a commercial source (Research Blood,

330 Boston) or anonymous donors from the French Bloodbank (Etablissement Français du Sang,

331 Pyrénées Méditerranée, France). Continuous culture was typically carried at 2-5%-hematocrit in

332 RPMI-1640 (Sigma Aldrich, Cat. No. R6504) supplemented with HEPES, 25 mM; Albumax II,

333 4.31 mg/ml (Thermo Fisher Scientific), or 10% human serum; sodium bicarbonate, 2.42 mM;

334 and gentamycin (20-25 µg/ml). Parasites were cultured at 37º C in hypoxic conditions (1-5% O_2,

335 5% CO_2, with N_2 as balance) in modular incubator chambers. Parasites were transfected by

336 electroporation (*94*), and treated with WR99210 (2.5-5 nM) or blasticidin (2.5 µg/ml).

337 *Pf*PP1-DD transfectants were further selected for single-crossover integrants by cycles of on-

338 drug and off-drug treatment (*10*, *95*). All transgenic lines were cloned by limiting dilution and

339 genotyped by PCR. Unless otherwise noted, all experiments with *Pf*PP1-DD parasites indicate a

340 line constructed in the D10 background.

341 We synchronized parasites with heparin (100 units/ml) to define restricted periods of invasion

342 (*96*). Alternatively, we isolated schizonts by magnetic-affinity purification (MACs LS column,

343 Miltenyi, fitted with a 23-gauge needle) or 70% Percoll cushion, and allowed invasion into

344 uninfected erythrocytes for a defined period. Following invasion, we either added heparin to

345   block further invasion, selectively lysed remaining schizonts by sorbitol treatment (5% w/v in

346   double-distilled water), or separated recently invaded rings from unruptured schizonts by

347   magnetic affinity purification (MACs LS with 27-gauge needle).

348   Statistical significance testing

349   We carried out all tests for statistical significance in Prism software (GraphPad). Unless

350   otherwise stated, *P*-values indicate the results of paired, two-tailed *t*-tests.

351   Induction of *Pf*PP1-phenotypes through conditional expression

352   For assays, we induced parasites for either knockout of *pfpp1* [mock- (DMSO) versus Rapa, 10

353   nM] or knockdown of *Pf*PP1-DD [Shld1 (0.2-0.5 µM) versus ethanol vehicle]. In knockout

354   parasites, we washed away Rapa 4 hrs following addition.

355   Immunoblot analysis

356   For immunoblot analysis, we released parasites from erythrocytes with cold PBS containing 0.1-

357   0.2% saponin, and boiled in SDS-PAGE sample buffer as previously described (*10*). Following

358   electrophoretic separation, proteins were transferred to a nitrocellulose membrane, and

359   immunoblot analysis was carried out using the LI-COR system (Lincoln, USA), or the Chemidoc

360   system (Bio-Rad).

361   Microscopy

362   *Light microscopy.* For quantitative assessment of nuclear centers in terminally developed

363   *Pf*PP1-DD parasites [~54-60 hpi; +E64 (50 µM) since ~45 hpi], we collected ~500,000 infected

364   cells onto glass slides by cytospin centrifugation, followed by fixation in methanol and staining

365   with May-Grünwald-Giemsa. All infected cells encountered in visual fields by conventional light

366   microscopy were counted, typically >80 per sample. In the *pfpp1-iKO* line, we used

17

367 immunofluorescence microscopy (see below) to identify segmented parasites that stained

368 positive for the antigen *Pf*MTIP before counting nuclei stained with DAPI. Immunofluorescence

369 analysis was carried out essentially as described (*97*). Thin smears were fixed in 4%-

370 paraformaldehyde in PBS for 10 minutes at room-temperature or overnight at 4º C in a

371 humidified chamber followed by extensive washing in buffer; permeabilized with 0.1%-Triton-

372 X-100/PBS for 10 minutes at room temperature before further washing; blocked with 3%

373 BSA/PBS for >1 hr at room temperature or overnight at 4º C; treated with primary antibody

374 overnight at 4º C; washed extensively before treatment with the appropriate Alexa-488

375 secondary antibody (1:1000 dilution) for 1 hr at room temperature; washed and prepared in

376 DAPI-containing mounting solution for imaging. Images were taken with a Zeiss Axioimager Z2

377 or AxioObserver.Z1, and processed with Zen blue edition software (Zeiss) or Fiji (*98*). For

378 immunofluorescence assays for PVM rupture or secretion of exoneme or microneme antigens,

379 parasites were treated at 41 hpi with 50 µM E64 and smeared 4-5 hrs later for analysis.

380 For assessment of TF-PtdC labeling of *P. falciparum*, we treated synchronous (+/-1 hr)

381 *Pf*PP1-DD parasites (+0.5 µM Shld1) with or without E64 (50 µM) for ~7 hrs before image

382 acquisition at the indicated timepoints. After evaporation of TF-PtdC on the surface of multiplate

383 wells, we added parasites in standard media (2%-hematocrit) for a final concentration of

384 fluorescent label of 100 µM. After ~30 minutes at 37º C in standard culture conditions, cells

385 were collected and stored at 4ºC until imaging carried out over the course of the next ~2 hrs. Just

386 before imaging, parasites were spotted and mixed with Hoechst dye on coverslips (No. 1.5) pre-

387 treated with Concanavalin-A (Sigma-Aldrich, Cat. No. C5275, 0.5 mg/ml in PBS; spread and

388 dried at 37º C for ~30 minutes) immediately before sealing by surface tension and dispersion of

389 cell suspension with a glass slide. Images were acquired with a 63x-objective on the Zeiss

390   Axioimager Z2 in the DIC, DAPI, and GFP channels. We scored 40-66 multinucleate, infected

391   cells per condition to estimate internal labeling of parasites.

392   *Transmission electron microscopy*. For *pfpp1-iKO* cells, we directly added 25% glutaraldehyde

393   (EM grade) to the culture medium to obtain a final concentration of 2.5%. After 10 min

394   incubation at room temperature, we centrifuged the cells and resuspended the pellet in 20

395   volumes of cacodylate buffer (0.1 M) containing 2.5% glutaraldehyde and 5 mM $CaCl_2$.The

396   suspension was left 2 hours at RT before long-term storage at 4°C in fixative until further

397   processing. All the following incubation steps were performed in suspension, followed by

398   centrifugation using a benchtop microcentrifuge. Cells were washed with cacodylate buffer and

399   post-fixed with 1% O_sO_4 and 1.5% potassium ferrocyanide in cacodylate buffer for 1 hr. After

400   washing with distilled water, samples were incubated overnight in 2% uranyl acetate in water

401   and dehydrated in graded series of acetonitrile. Impregnation in Epon 812 was performed in

402   suspension on a rotary shaker for 1hr in Epon: acetonitrile (1:1) and 2x 1hr in 100% Epon. After

403   the last step, cells were pelleted in fresh epon and polymerized for 48 hrs at 60° C. 70 nm

404   sections were made with an ultramicrotome Leica UC7, contrasted with uranyl acetate and lead

405   citrate and imaged for transmission electron microscopy (TEM) on a JEOL 1200 EX. All

406   chemicals were purchased from Electron Microscopy Sciences (USA).

407   TEM analysis of *Pf*PP1-DD parasites was carried out similarly, with some modifications. For

408   fixation, 1 volume of suspended culture (> ~5 µl packed cell volume) was supplemented with 1

409   volume of a 2x fixative solution (5% glutaraldehyde, 2.5% paraformaldehyde, 0.06% picric acid

410   in 0.2M cacodylate buffer, pH 7.4), spun briefly at 500g, and stored at 4° C before further

411   processing. Following fixation, cells were washed in water, then maleate buffer before

412   incubation in 2% uranyl acetate (1 hr). Following washes in water, dehydration was done in

413   grades of alcohol (10 min each at 50%, 70%, 90%, and 2x 100%). The samples were then put in

414   propyleneoxide for 1 hr and infiltrated overnight in a 1:1 mixture of propyleneoxide and TAAB

415   Epon (Marivac Canada Inc. St. Laurent, Canada). The following day, the samples were

416   embedded in TAAB Epon and polymerized at 60º C for 48 hrs. Ultrathin sections (about 60nm)

417   were cut on a Reichert Ultracut-S microtome, picked up on to copper grids stained with lead

418   citrate and examined in a JEOL 1200EX or a TecnaiG² Spirit BioTWIN. Images were recorded

419   with an AMT 2k CCD camera.

420   <u>Flow-cytometry and analysis</u>

421   All measurements of parasitemia through flow-cytometry were carried out with staining of fixed

422   cells with SYBR-Green I (Invitrogen) to distinguish DNA-containing parasitized erythrocytes

423   from uninfected, enucleate erythrocytes (*10*, *13*, *99*, *100*). Fixation of *Pf*PP1-DD cell suspension

424   was carried out by addition of >3 volumes of PBS supplemented with paraformaldehyde (4%

425   final concentration) and glutaraldehyde (0.0075-0.015% final concentration), followed by

426   storage at 4º C for >12 hrs before further washes in buffer. For quantitative measurements of

427   cellular DNA, fixed cells were permeabilized with Triton-X-100 (0.1%) and RNase-treated (~0.3

428   mg/ml) before staining (*13*). For *pfpp1-iKO* parasites, cells were fixed by addition of an equal

429   volume of PBS-paraformaldehyde (8%); fluorescence was measured with a BD FACS Canto I

430   cytometer. For *Pf*PP1-DD parasites, flow-cytometry was carried out with a MacsQUANT

431   (Miltenyi) on the FITC channel. All flow-cytometry data were analyzed with FlowJo software.

432   To calculate cellular DNA content, we used fluorescence measurements from uninfected

433   erythrocytes (zero genomes), singly-infected rings (1 genome), and doubly-infected rings (2

434   genomes), to build standard curves for translation of total fluorescence of an infected erythrocyte

435   population into "genome equivalents." In some measurements, we applied a background

436 correction across all samples to subtract the contribution of parasite cells that did not advance

437 into DNA replication by 48-hpi (i.e. in +Shld1-conditions). To calculate egress from parasites

438 late in the IDC in an experiment, we used the remaining schizont populations measured at the

439 end of an assay. We treated schizont levels in No-Shld1 conditions (or 50 nM Shld1, fig. S5E,H)

440 as a measure of no-egress (zero), and levels with high-Shld1 as full egress (100%). We similarly

441 calculated egress-to-invasion from parasites late in the IDC using ring-stage parasite levels.

442 Fold-change in egress, as reported in Fig. 4, is the quotient of schizont levels at the end of the

443 assay in the absence of chemical (numerator) to schizonts levels left in the presence of chemical

444 (denominator).

445 <u>Proteomic and phosphoproteomic profiling</u>

446 *Parasite collection and processing for downstream analysis.* Proteomic and phosphoproteomic

447 analysis was carried out as described (*13*, *101*), with modifications. *Pf*PP1-DD parasites were

448 synchronized as described above using MACs purification of schizonts and was treated with

449 sorbitol (5% w/v in water) after 1.5 hours of invasion into uninfected erythrocytes to eliminate

450 remaining schizonts and isolate freshly re-invaded rings. Approximately 10×10^{10} synchronous

451 ring-stage *Pf*PP1-HA-DD parasites in Shld1 (0.3 μM) were cultured to 44 hpi with a preceding

452 change of warm media at ~24 hpi, washed extensively and replated in warm (37° C) complete-

453 RPMI at ~5×10^6 parasitized erythrocytes per ml of culture +/-0.3 μM Shld1. At 48 hpi, for each

454 Shld1 condition, 2 technical replicates each with or without Shld1 (~1×10^{10} parasitized

455 erythrocytes per replicate) were centrifuged at room temperature (500 g), and the pellet was

456 frozen at -80° C for downstream processing. Remaining cultures (3 technical replicates, each

457 with or without Shld1) were supplemented with E64 (15 μM) for further culture until 55 hpi for

458 collection as described above.

459   Further protein extraction steps for each of 10 samples were carried out in solutions

460   supplemented with cOmplete protease inhibitors (Roche) and PhosSTOP phosphatase inhibitor

461   cocktail (Roche). We released parasites with 0.05% saponin in PBS administered over several

462   washes, for a total of ~6.5 volumes of buffer for 1 packed erythrocyte volume of frozen pellet.

463   Following additional washes in PBS without saponin, we added >1 volume of 8 M urea lysis

464   buffer (100 mM NaCl, 25 mM Tris-HCl/pH 8), and subjected each sample to 5x freeze (-80ºC)-

465   thaw cycles before centrifugation at room temperature to separate protein-containing supernatant

466   from pelleted cellular debris. Yields for each of the 10 samples ranged from 5-7 mg as assessed

467   with the Pierce BCA (Bicinchoninic acid) protein assay. We reduced disulfide bonds with 5 mM

468   tris(2-chloroethyl) phosphate (TCEP) for 30 min at room temperature, alkylated cysteines with

469   15 mM iodoacetamide for 30 min at room temperature in the dark, and quenched excess

470   iodoacetamide by treatment with 5 mM dithiothreitol (DTT) for 15 min at room temperature. We

471   precipitated protein in chloroform-methanol (*102*) before resuspension (8 M urea, 50 mM

472   HEPES pH 8.5) and before dilution of urea to 1 M (50 mM HEPES pH 8.5) for digestion with

473   LysC protease (1:100 protease-to-protein ratio, 3 h at 37 °C) before the addition of trypsin (1:100

474   protease-to-protein ratio) and continued digestion overnight at 37 °C. We quenched the reaction

475   with 1% formic acid, carried out C18 solid-phase extraction (Sep-Pak, Waters), and precipitated

476   peptides with vacuum-centrifugation.

477   *Isobaric labeling with tandem mass tags (TMTs).* 200 µg of peptides from each sample was

478   dissolved in Buffer 1 (100 mM HEPES, pH 8.5). We carried out labelling with TMT reagents as

479   previously described (*103*), according to manufacturer instructions (Thermo-Fisher Scientific).

480   Following combination of the 10 TMT-labeled samples to match protein mass between samples,

481 the mixture was vacuum-centrifuged and subjected to C18 solid-phase extraction (Sep-Pak,

482 Waters) and eluate was collected.

483 *Phosphopeptide enrichment*. Peptides were resuspended in Buffer 1, followed by enrichment of

484 phosphopeptides with "High-Select™ Fe-NTA Phosphopeptide Enrichment Kit" (Thermo-

485 Scientific Cat. No. A32992) (*104*). The flow-through was retained for analysis of the proteome.

486 Peptides and enriched phosphopeptides were dried by vacuum centrifugation.

487 *Offline basic pH reversed-phase (BPRP) fraction*. For proteomic analysis, the TMT-labeled

488 peptide pool was fractionated via BPRP high-performance liquid chromatography (*103*). Eluted

489 fractions were desalted, dried by vacuum-centrifugation, and resuspended in a solution of 5%

490 acetonitrile and 5% formic acid, for mass spectrometry-based measurements.

491 For phosphopeptide analysis, we used the Pierce Off-line BPRP fractionation kit (Thermo

492 Scientific), collecting and processing fractions for LC-MS/MS-based analysis as described

493 previously (*13*).

494 *Liquid chromatography and tandem mass spectrometry*. We collected MS/MS data using an

495 Orbitrap Fusion mass spectrometer (Thermo Fisher Scientific) coupled to a Proxeon EASY-nLC

496 1000 liquid chromatography (LC) pump (Thermo Fisher Scientific). For each analysis, 1 μg

497 protein was loaded onto the LC onto an in-house pulled C18 column [30-35 cm, 2.6 um

498 Accucore (Thermo Fisher), 100um ID] for MS-analysis (*13*).

499 Global proteome and phosphoproteome analyses each employed the multi-notch MS3-based

500 method (*13*, *105*). Global proteome and phosphoproteome analyses used an MS3-based TMT

501 method (*106*, *107*), which has been shown to reduce ion interference compared to MS2

502 quantification (*108*).

23

503   *Mass spectrometry data analysis*. Mass spectra were analyzed with a SEQUEST-based pipeline

504   (*13*, *109*). Peptide spectral matches (PSMs) were carried out a 1% false discovery rate (FDR),

505   and filtered as previously described with minor modifications (*13*). To quantify the TMT-

506   reporter ion, in each channel (0.003 Th range to distinguish reporters) we extracted the summed

507   signal-to-noise (S/N) ratio and found the closest matching centroid to the expected mass. For

508   proteomic analysis, PSMs (1% FDR) were collapsed to whole proteins (1% FDR). We used

509   principles of parsimony to assemble the protein set, aiming to identify the smallest number of

510   distinct polypeptides required to explain the observed PSMs. Relative protein levels were

511   quantified by calculating the sum of reporter ion counts across associated PSMs (*109*). MS3

512   spectra represented in <2 TMT channels, and MS3 spectra with TMT reporter summed spectra of

513   <100, or no MS3 spectra, were not considered for further analysis (*105*). Protein quantitation

514   values were exported to Microsoft Excel. To normalize for variations in sample loading, within

515   each TMT reporter ion channel, each parasite protein was normalized to the total signal of the *P.*

516   *falciparum* proteome measured in that channel (*13*). For phosphoproteomics, the level of each

517   phosphopeptide in a single TMT channel was normalized to the level of the parent protein in the

518   same experimental conditions (i.e. average of normalized values for technical replicate

519   measurements from proteomics). We did not apply this adjustment for the <2% of

520   phosphopeptides that could not be mapped to a parent protein in proteomics.

521   *Gene Ontology analysis of proteins upregulated with PfPP1-knockdown*. For the 19 proteins

522   shown to be increased in expression (>1.3-fold) in two proteomics measurements from separate

523   experiments (Tables S1 and S2), we carried out gene ontology enrichment analysis using the

524   webtool at PlasmoDB (http://www.plasmodb.org). The 10 most enriched GO categories are

525   shown in Table S4.

526 *Prioritization of late IDC-stage genes.* For restriction of candidate substrates of *Pf*PP1 to

527 proteins expressed late in the IDC, we used web-based tools at PlasmoDB

528 (https://www.plasmodb.org) relying on published transcriptome data (*30*) to identify *P.*

529 *falciparum* genes that are upregulated at the 40- or 48 hpi-mark of the IDC by at least 3-fold over

530 levels at the midpoint of the IDC (average expression of 16 and 24 hpi), and by at least 1.5-fold

531 over levels at 32 hpi.

532 <u>Chemical genetic assays</u>

533 Compounds in DMSO (10 mM) were printed onto the surface of standard 96-well plates, using a

534 D300e automated dispenser (Hewlett Packard), and stored at -20º C until addition of parasites.

535 Chemicals in water were added individually onto the surface of 96-well plates, or added directly

536 at the high concentration to parasites in wells before serial dilution in-plate. Phospholipids (or

537 methanol vehicle) at 10x final concentration were added to the surface of plates and allowed to

538 evaporate before addition of parasites. Synchronized *Pf*PP1-DD parasites were washed

539 extensively in media without Shld1 and supplemented with varying concentrations of Shld1

540 (constant volume of ethanol carrier across doses), as indicated in the data. Parasites with Shld1,

541 set at 0.5%-hematocrit, were added at 100 µl volume to wells with compounds to attain the

542 reported final concentrations. Wells immediately surrounding the samples were filled with water

543 or aqueous solution to prevent evaporation through the course of the assay. Parasites were

544 allowed to incubate with inhibitor for ~20 hrs before fixation and measurement of egress from

545 schizonts and reinvasion to rings by flow-cytometry.

546 <u>Data availability</u>

547 All data are available in the manuscript or supplementary materials.

548

Referencess

1. N. Gerald, B. Mahajan, S. Kumar, Mitosis in the Human Malaria Parasite Plasmodium falciparum. *Eukaryotic Cell*. **10**, 474–482 (2011).

2. D. E. Arnot, E. Ronander, D. C. Bengtsson, The progression of the intra-erythrocytic cell cycle of Plasmodium falciparum and the role of the centriolar plaques in asynchronous mitotic division during schizogony. *International Journal for Parasitology*. **41**, 71–80 (2011).

3. M. E. Francia, B. Striepen, Cell division in apicomplexan parasites. *Nat Rev Micro*. **12**, 125–136 (2014).

4. B. N. Pease *et al.*, Global Analysis of Protein Expression and Phosphorylation of Three Stages of Plasmodium falciparumIntraerythrocytic Development. *J. Proteome Res.* **12**, 4028–4045 (2013).

5. E. Bushell *et al.*, Functional Profiling of a Plasmodium Genome Reveals an Abundance of Essential Genes. *Cell*. **170**, 260–272 (2017).

6. M. Zhang *et al.*, Uncovering the essential genes of the human malaria parasite Plasmodium falciparumby saturation mutagenesis. *Science*. **360**, eaap7847–30 (2018).

7. R. Tewari *et al.*, The Systematic Functional Analysis of Plasmodium Protein Kinases Identifies Essential Regulators of Mosquito Transmission. *Cell Host & Microbe*. **8**, 377–387 (2010).

8. D. S. Guttery *et al.*, Genome-wide Functional Analysis of Plasmodium Protein Phosphatases Reveals Key Regulators of Parasite Development and Differentiation. *Cell Host & Microbe*. **16**, 128–140 (2014).

571   9.   H. M. Taylor *et al.*, The Malaria Parasite Cyclic GMP-Dependent Protein Kinase Plays a

572   Central Role in Blood-Stage Schizogony. *Eukaryotic Cell*. **9**, 37–45 (2010).

573   10.   A. S. Paul *et al.*, Parasite Calcineurin Regulates Host Cell Recognition and Attachment by

574   Apicomplexans. *Cell Host & Microbe*. **18**, 49–60 (2015).

575   11.   J. D. Dvorin *et al.*, A Plant-Like Kinase in Plasmodium falciparum Regulates Parasite

576   Egress from Erythrocytes. *Science*. **328**, 910–912 (2010).

577   12.   L. Solyakov *et al.*, Global kinomic and phospho-proteomic analyses of the human malaria

578   parasite Plasmodium falciparum. *Nature Communications*. **2**, 565 (2011).

579   13.   M. Ganter *et al.*, Plasmodium falciparum CRK4 directs continuous rounds of DNA

580   replication during schizogony. *Nature Microbiology*. **2**, 17017 (2017).

581   14.   A. Patel *et al.*, Cyclic AMP signalling controls key components of malaria parasite host cell

582   invasion machinery. *PLoS Biol*. **17**, e3000264 (2019).

583   15.   M. M. Alam *et al.*, Validation of the protein kinase PfCLK3 as a multistage cross-species

584   malarial drug target. *Science*. **365**, eaau1682–10 (2019).

585   16.   L. Reininger, J. M. Wilkes, H. Bourgade, D. Miranda-Saavedra, C. Doerig, An essential

586   Aurora-related kinase transiently associates with spindle pole bodies during Plasmodium

587   falciparum erythrocytic schizogony. *Molecular Microbiology*. **79**, 205–221 (2010).

588   17.   C. Wurzenberger, D. W. Gerlich, Phosphatases: providing safe passage through mitotic

589   exit. *Nat Rev Mol Cell Biol*. **12**, 469–482 (2011).

590   18.   M. Bollen, D. W. Gerlich, B. Lesage, Mitotic phosphatases: from entry guards to exit

591   guides. *Trends in Cell Biology*. **19**, 531–541 (2009).

592   19.   N. T. L. Rodrigues *et al.*, Kinetochore-localized PP1–Sds22 couples chromosome

593   segregation to polar relaxation. *Nature*. **524**, 489–492 (2015).

594   20.   H. Ohkura, N. Kinoshita, S. Miyatani, T. Toda, M. Yanagida, The fission yeast dis2+ gene

595   required for chromosome disjoining encodes one of two putative type 1 protein

596   phosphatases. *Cell*. **57**, 997–1007 (1989).

597   21.   I. Sassoon *et al.*, Regulation of Saccharomyces cerevisiae kinetochores by the type 1

598   phosphatase Glc7p. *Genes & Development*. **13**, 545–555 (1999).

599   22.   H. Ceulemans, M. Bollen, Functional Diversity of Protein Phosphatase-1, a Cellular

600   Economizer and Reset Button. *Physiological Reviews*. **84**, 1–39 (2004).

601   23.   P. Cohen, D. L. Schelling, M. J. Stark, Remarkable similarities between yeast and

602   mammalian protein phosphatases. *FEBS Letters*. **250**, 601–606 (1989).

603   24.   P. Cohen, S. Klumpp, D. L. Schelling, An improved procedure for identifying and

604   quantitating protein phosphatases in mammalian tissues. *FEBS Letters*. **250**, 596–600

605   (1989).

606   25.   C. MacKintosh, P. Cohen, Identification of high levels of type 1 and type 2A protein

607   phosphatases in higher plants. *Biochem. J.* **262**, 335–339 (1989).

608   26.   A. T. Sim, E. Ratcliffe, M. C. Mumby, E. Villa-Moruzzi, J. A. Rostas, Differential

609   activities of protein phosphatase types 1 and 2A in cytosolic and particulate fractions from

610   rat forebrain. *J. Neurochem.* **62**, 1552–1559 (1994).

611   27.   R. Kumar, B. Adams, A. Oldenburg, A. Musiyenko, S. Barik, Characterisation and

612   expression of a PP1 serine/threonine protein phosphatase (PfPP1) from the malaria

parasite, Plasmodium falciparum: demonstration of its essential role using RNA interference. *Malar J*. **1**, 5 (2002).

28. M. Zhang, S. Mishra, R. Sakthivel, B. M. A. Fontoura, V. Nussenzweig, UIS2: A Unique Phosphatase Required for the Development of Plasmodium Liver Stages. *PLoS Pathog*. **12**, e1005370–20 (2016).

29. R. Bártfai *et al.*, H2A.Z Demarcates Intergenic Regions of the Plasmodium falciparum Epigenome That Are Dynamically Marked by H3K9ac and H3K4me3. *PLoS Pathog*. **6**, e1001223–14 (2010).

30. T. D. Otto *et al.*, New insights into the blood-stage transcriptome of Plasmodium falciparum using RNA-Seq. *Molecular Microbiology*. **76**, 12–24 (2010).

31. G. Tellier *et al.*, Identification of Plasmodium falciparum Translation Initiation eIF2β Subunit: Direct Interaction with Protein Phosphatase Type 1. *Front. Microbiol*. **7**, 429–16 (2016).

32. A. Lenne *et al.*, Characterization of a Protein Phosphatase Type-1 and a Kinase Anchoring Protein in Plasmodium falciparum. *Front. Microbiol*. **9**, 2617 (2018).

33. B. Gnangnon *et al.*, Plasmodium pseudo-Tyrosine Kinase-like binds PP1 and SERA5 and is exported to host erythrocytes. *Sci Rep*. **9**, 8120 (2019).

34. T. Hollin, C. De Witte, A. Lenne, C. Pierrot, J. Khalife, Analysis of the interactome of the Ser/Thr Protein Phosphatase type 1 in Plasmodium falciparum. *BMC Genomics*. **17**, 246 (2016).

35. T. Hollin *et al.*, Essential role of GEXP15, a specific Protein Phosphatase type 1 partner, in Plasmodium berghei in asexual erythrocytic proliferation and transmission. *PLoS Pathog*. **15**, e1007973–32 (2019).

36. A. Fréville *et al.*, Plasmodium falciparum inhibitor-3 homolog increases protein phosphatase type 1 activity and is essential for parasitic survival. *J. Biol. Chem.* **287**, 1306–1321 (2012).

37. A. Fréville *et al.*, Identification of a Plasmodium falciparuminhibitor-2 motif involved in the binding and regulation activity of protein phosphatase type 1. *FEBS Journal*. **281**, 4519–4534 (2014).

38. A. Fréville *et al.*, Plasmodium falciparum encodes a conserved active inhibitor-2 for Protein Phosphatase type 1: perspectives for novel anti-plasmodial therapy. *BMC Biol*. **11**, 80 (2013).

39. W. Daher *et al.*, Regulation of protein phosphatase type 1 and cell cycle progression by PfLRR1, a novel leucine-rich repeat protein of the human malaria parasite Plasmodium falciparum. *Molecular Microbiology*. **60**, 578–590 (2006).

40. A. Bloecher, K. Tatchell, Dynamic localization of protein phosphatase type 1 in the mitotic cell cycle of Saccharomyces cerevisiae. *J Cell Biol*. **149**, 125–140 (2000).

41. E. Knuepfer, M. Napiorkowska, C. van Ooij, A. A. Holder, Generating conditional gene knockouts in Plasmodium – a toolkit to produce stable DiCre recombinase-expressing parasite lines using CRISPR/Cas9. *Sci Rep*. **7**, 1–12 (2017).

42. C. R. Collins *et al.*, Robust inducible Cre recombinase activity in the human malaria parasite Plasmodium falciparumenables efficient gene deletion within a single asexual erythrocytic growth cycle. *Molecular Microbiology*. **88**, 687–701 (2013).

43. L. A. Banaszynski, L.-C. Chen, L. A. Maynard-Smith, A. G. L. Ooi, T. J. Wandless, A Rapid, Reversible, and Tunable Method to Regulate Protein Function in Living Cells Using Synthetic Small Molecules. *Cell*. **126**, 995–1004 (2006).

44. C. M. Armstrong, D. E. Goldberg, An FKBP destabilization domain modulates protein levels in Plasmodium falciparum. *Nat Meth*. **4**, 1007–1009 (2007).

45. S. Yeoh *et al.*, Subcellular Discharge of a Serine Protease Mediates Release of Invasive Malaria Parasites from Host Erythrocytes. *Cell*. **131**, 1072–1083 (2007).

46. J. A. Thomas *et al.*, A protease cascade regulates release of the human malaria parasite Plasmodium falciparum from host red blood cells. *Nature Microbiology*. **3**, 447–455 (2018).

47. C. R. Collins *et al.*, Malaria Parasite cGMP-dependent Protein Kinase Regulates Blood Stage Merozoite Secretory Organelle Discharge and Egress. *PLoS Pathog*. **9**, e1003344–13 (2013).

48. S. Glushakova *et al.*, Rounding precedes rupture and breakdown of vacuolar membranes minutes before malaria parasite egress from erythrocytes. *Cellular Microbiology*. **20**, e12868–12 (2018).

49. J. Lehár, B. R. Stockwell, G. Giaever, C. Nislow, Combination chemical genetics. *Nat Chem Biol*. **4**, 674–681 (2008).

674   50.   D. Yokoyama *et al.*, Modulation of the growth of Plasmodium falciparum in vitro by

675   protein serine/threonine phosphatase inhibitors. *Biochemical and Biophysical Research*

676   *Communications*. **247**, 18–23 (1998).

677   51.   M. Swingle, L. Ni, R. E. Honkanen, "Small-Molecule Inhibitors of Ser/Thr Protein

678   Phosphatases: Specificity, Use and Common Forms of Abuse" in *Methods Mol Biol.*

679   (Humana Press, New Jersey, 2006), vol. 365, pp. 23–38.

680   52.   M. Treeck, J. L. Sanders, J. E. Elias, J. C. Boothroyd, The Phosphoproteomes of

681   Plasmodium falciparum and Toxoplasma gondii Reveal Unusual Adaptations Within and

682   Beyond the Parasites' Boundaries. *Cell Host & Microbe*. **10**, 410–419 (2011).

683   53.   B. N. Pease *et al.*, Characterization of Plasmodium falciparum Atypical Kinase PfPK7–

684   Dependent Phosphoproteome. *J. Proteome Res.* **17**, 2112–2123 (2018).

685   54.   M. M. Alam *et al.*, Phosphoproteomics reveals malaria parasite Protein Kinase G as a

686   signalling hub regulating egress and invasion. *Nature Communications*. **6**, 7285 (2015).

687   55.   S. Kumar *et al.*, PfCDPK1 mediated signaling in erythrocytic stages of Plasmodium

688   falciparum. *Nature Communications*. **8**, 63 (2017).

689   56.   J. F. Cannon, *"Function of Protein Phosphatase-1, Glc7, in Saccharomyces cerevisiae"* in

690   *Advances in Applied Microbiology* (Elsevier, Burlington, 2010), vol. 73, pp. 27-59.

691   57.   W. Wang, P. T. Stukenberg, D. L. Brautigan, Phosphatase inhibitor-2 balances protein

692   phosphatase 1 and aurora B kinase for chromosome segregation and cytokinesis in human

693   retinal epithelial cells. *Mol. Biol. Cell*. **19**, 4852–4862 (2008).

694   58.   M. W. Peggie *et al.*, Essential functions of Sds22p in chromosome stability and nuclear

695   localization of PP1. *Journal of Cell Science*. **115**, 195–206 (2002).

59. H. Y. Tung, W. Wang, C. S. Chan, Regulation of chromosome segregation by Glc8p, a structural homolog of mammalian inhibitor 2 that functions as both an activator and an inhibitor of yeast protein phosphatase 1. *Molecular and Cellular Biology*. **15**, 6064–6074 (1995).

60. J. E. Salcedo-Sora, E. Caamano-Gutierrez, S. A. Ward, G. A. Biagini, The proliferating cell hypothesis: a metabolic framework for Plasmodium growth and development. *Trends in Parasitology*. **30**, 170–175 (2014).

61. H. Goto, Y. Yasui, E. A. Nigg, M. Inagaki, Aurora-B phosphorylates Histone H3 at serine28 with regard to the mitotic chromosome condensation. *Genes Cells*. **7**, 11–17 (2002).

62. I. J. de Castro *et al.*, Repo-Man/PP1 regulates heterochromatin formation in interphase. *Nature Communications*. **8**, 14048 (2017).

63. T. Mund, M. J. Lewis, S. Maslen, H. R. Pelham, Peptide and small molecule inhibitors of HECT-type ubiquitin ligases. *Proceedings of the National Academy of Sciences*. **111**, 16736–16741 (2014).

64. D. J. Carucci *et al.*, Guanylyl Cyclase Activity Associated with Putative Bifunctional Integral Membrane Proteins in Plasmodium falciparum. *J. Biol. Chem.* **275**, 22147–22156 (2000).

65. H. Bisio, M. Lunghi, M. Brochet, D. Soldati-Favre, Phosphatidic acid governs natural egress in Toxoplasma gondii via a guanylate cyclase receptor platform. *Nature Microbiology*. **4**, 420–428 (2019).

717   66.   K. M. Brown, L. D. Sibley, Essential cGMP Signaling in Toxoplasma Is Initiated by a

718   Hybrid P-Type ATPase-Guanylate Cyclase. *Cell Host & Microbe*. **24**, 804–816 (2018).

719   67.   Ö. Günay-Esiyok, U. Scheib, M. Noll, N. Gupta, An unusual and vital protein with

720   guanylate cyclase and P4-ATPase domains in a pathogenic protist. *Life Sci. Alliance*. **2**,

721   e201900402–19 (2019).

722   68.   L. Yang *et al.*, An apically located hybrid guanylate cyclase–ATPase is critical for the

723   initiation of Ca 2+signaling and motility in Toxoplasma gondii. *J. Biol. Chem.* **294**, 8959–

724   8972 (2019).

725   69.   W. J. Thompson, Cyclic nucleotide phosphodiesterases: pharmacology, biochemistry and

726   function. *Pharmacol. Ther.* **51**, 13–33 (1991).

727   70.   K. Yuasa *et al.*, PfPDE1, a novel cGMP-specific phosphodiesterase from the human

728   malaria parasite Plasmodium falciparum. *Biochem. J.* **392**, 221–229 (2005).

729   71.   M. Brochet *et al.*, Phosphoinositide Metabolism Links cGMP-Dependent Protein Kinase G

730   to Essential Ca2+ Signals at Key Decision Points in the Life Cycle of Malaria Parasites.

731   *PLoS Biol.* **12**, e1001806–15 (2014).

732   72.   D. A. Baker *et al.*, Cyclic nucleotide signalling in malaria parasites. *Open Biol.* **7**, 170213–

733   18 (2017).

734   73.   R. K. Sah, S. Garg, P. Dangi, K. Ponnusamy, S. Singh, Phosphatidic acid homeostasis

735   regulated by a type-2 phosphatidic acid phosphatase represents a novel druggable target in

736   malaria intervention. *Cell Death Discovery*. **5,** 107 (2019).

737   74.   H. E. Bullen *et al.*, Phosphatidic Acid-Mediated Signaling Regulates Microneme Secretion

738   in Toxoplasma. *Cell Host & Microbe.* **19**, 349–360 (2016).

75. H. Hidaka *et al.*, Specific, rapid, and sensitive enzymatic measurement of sphingomyelin, phosphatidylcholine and lysophosphatidylcholine in serum and lipid extracts. *Clinical Biochemistry*. **41**, 1211–1217 (2008).

76. M. R. Hojjati, X.-C. Jiang, Rapid, specific, and sensitive measurements of plasma sphingomyelin and phosphatidylcholine. *J. Lipid Res.* **47**, 673–676 (2006).

77. D. Jacot *et al.*, An Apicomplexan Actin-Binding Protein Serves as a Connector and Lipid Sensor to Coordinate Motility and Invasion. *Cell Host & Microbe*. **20**, 731–743 (2016).

78. N. M. B. Brancucci *et al.*, Lysophosphatidylcholine Regulates Sexual Stage Differentiation in the Human Malaria Parasite Plasmodium falciparum. *Cell*. **171**, 1532–1544 (2017).

79. S. Wein *et al.*, Contribution of the precursors and interplay of the pathways in the phospholipid metabolism of the malaria parasite. *J. Lipid Res.* **59**, 1461–1471 (2018).

80. B. Peter-Riesch, M. Fathi, W. Schlegel, C. B. Wollheim, Glucose and carbachol generate 1,2-diacylglycerols by different mechanisms in pancreatic islets. *J. Clin. Invest.* **81**, 1154–1161 (1988).

81. S. Glushakova *et al.*, New Stages in the Program of Malaria Parasite Egress Imaged in Normal and Sickle Erythrocytes. *Current Biology*. **20**, 1117–1121 (2010).

82. C. R. Collins, F. Hackett, J. Atid, M. S. Y. Tan, M. J. Blackman, The Plasmodium falciparum pseudoprotease SERA5 regulates the kinetics and efficiency of malaria parasite egress from host erythrocytes. *PLoS Pathog*. **13**, e1006453–32 (2017).

83. V. L. Hale *et al.*, Parasitophorous vacuole poration precedes its rupture and rapid host erythrocyte cytoskeleton collapse in Plasmodium falciparum egress. *Proceedings of the National Academy of Sciences*. **114**, 3439–3444 (2017).

761   84.   P. I. Holm, P. M. Ueland, G. Kvalheim, E. A. Lien, Determination of choline, betaine, and

762   dimethylglycine in plasma by a high-throughput method based on normal-phase

763   chromatography-tandem mass spectrometry. *Clin. Chem.* **49**, 286–294 (2003).

764   85.   C. J. Taylor, L. McRobert, D. A. Baker, Disruption of a Plasmodium falciparum cyclic

765   nucleotide phosphodiesterase gene causes aberrant gametogenesis. *Molecular*

766   *Microbiology.* **69**, 110–118 (2008).

767   86.   R. W. Moon *et al.*, A Cyclic GMP Signalling Module That Regulates Gliding Motility in a

768   Malaria Parasite. *PLoS Pathog.* **5**, e1000599–14 (2009).

769   87.   V. Lakshmanan *et al.*, Cyclic GMP Balance Is Critical for Malaria Parasite Transmission

770   from the Mosquito to the Mammalian Host. *mBio.* **6**, e02330 (2015).

771   88.   A. Flammersfeld, C. Lang, A. Flieger, G. Pradel, Phospholipases during membrane

772   dynamics in malaria parasites. *International Journal of Medical Microbiology.* **308**, 129–

773   141 (2018).

774   89.   N. Roger *et al.*, Characterization of a 225 kilodalton rhoptry protein of Plasmodium

775   falciparum. *Molecular and Biochemical Parasitology.* **27**, 135–141 (1988).

776   90.   D. A. Holt, J. I. Luengo, D. S. Yamashita, H. O. J. O. the, 1993, Design, synthesis, and

777   kinetic evaluation of high-affinity FKBP ligands and the X-ray crystal structures of their

778   complexes with FKBP12. *ACS Publications.* **115**, 9925–9938 (1993).

779   91.   W. Yang *et al.*, Investigating Protein−Ligand Interactions with a Mutant FKBP Possessing

780   a Designed Specificity Pocket. *J. Med. Chem.* **43**, 1135–1142 (2000).

92. L. J. Nkrumah *et al.*, Efficient site-specific integration in Plasmodium falciparum chromosomes mediated by mycobacteriophage Bxb1 integrase. *Nat Meth*. **3**, 615–621 (2006).

93. W. Trager, J. B. Jensen, Human malaria parasites in continuous culture. *Science*. **193**, 673–675 (1976).

94. D. A. Fidock, T. E. Wellems, Transformation with human dihydrofolate reductase renders malaria parasites insensitive to WR99210 but does not affect the intrinsic activity of proguanil. *Proceedings of the National Academy of Sciences*. **94**, 10931–10936 (1997).

95. T. Triglia, P. Wang, P. F. Sims, J. E. Hyde, A. F. Cowman, Allelic exchange at the endogenous genomic locus in Plasmodium falciparum proves the role of dihydropteroate synthase in sulfadoxine-resistant malaria. *The EMBO Journal*. **17**, 3807–3815 (1998).

96. M. J. Boyle *et al.*, Isolation of viable Plasmodium falciparum merozoites to define erythrocyte invasion events and advance vaccine and drug development. *Proceedings of the National Academy of Sciences*. **107**, 14378–14383 (2010).

97. S. Absalon *et al.*, Calcium-Dependent Protein Kinase 5 Is Required for Release of Egress-Specific Organelles in Plasmodium falciparum. *mBio*. **9**, 411–16 (2018).

98. J. Schindelin *et al.*, Fiji: an open-source platform for biological-image analysis. *Nat Meth*. **9**, 676–682 (2012).

99. A. K. Bei *et al.*, A flow cytometry-based assay for measuring invasion of red blood cells by Plasmodium falciparum. *Am. J. Hematol.* **85**, 234–237 (2010).

100. A. Farrell *et al.*, A DOC2 Protein Identified by Mutational Profiling Is Essential for Apicomplexan Parasite Exocytosis. *Science*. **335**, 218–221 (2012).

101. J. Navarrete-Perea, Q. Yu, S. P. Gygi, J. A. Paulo, Streamlined Tandem Mass Tag (SL-TMT) Protocol: An Efficient Strategy for Quantitative (Phospho)proteome Profiling Using Tandem Mass Tag-Synchronous Precursor Selection-MS3. *J. Proteome Res.* **17**, 2226–2236 (2018).

102. D. Wessel, U. I. Flügge, A method for the quantitative recovery of protein in dilute solution in the presence of detergents and lipids. *Analytical Biochemistry*. **138**, 141–143 (1984).

103. J. A. Paulo, S. P. Gygi, A comprehensive proteomic and phosphoproteomic analysis of yeast deletion mutants of 14-3-3 orthologs and associated effects of rapamycin. *Proteomics*. **15**, 474–486 (2015).

104. J. A. Paulo, J. Navarrete-Perea, A. R. Erickson, J. Knott, S. P. Gygi, An Internal Standard for Assessing Phosphopeptide Recovery from Metal Ion/Oxide Enrichment Strategies. *Journal of The American Society for Mass Spectrometry*. **29**, 1505–1511 (2018).

105. G. C. McAlister *et al.*, Increasing the Multiplexing Capacity of TMTs Using Reporter Ion Isotopologues with Isobaric Masses. *Anal. Chem.* **84**, 7469–7478 (2012).

106. L. Ting, R. Rad, S. P. Gygi, W. Haas, MS3 eliminates ratio distortion in isobaric multiplexed quantitative proteomics. *Nat Meth*. **8**, 937–940 (2011).

107. G. C. McAlister *et al.*, MultiNotch MS3 Enables Accurate, Sensitive, and Multiplexed Detection of Differential Expression across Cancer Cell Line Proteomes. *Anal. Chem.* **86**, 7150–7158 (2014).

108. J. A. Paulo, J. D. O'Connell, S. P. Gygi, A Triple Knockout (TKO) Proteomics Standard for Diagnosing Ion Interference in Isobaric Labeling Experiments. *Journal of The American Society for Mass Spectrometry*. **27**, 1620–1625 (2016).

38

825   109. E. L. Huttlin *et al.*, A Tissue-Specific Atlas of Mouse Protein Phosphorylation and

826   Expression. *Cell*. **143**, 1174–1189 (2010).

827   110. B. M. Invergo *et al.*, Sub-minute Phosphoregulation of Cell Cycle Systems during

828   Plasmodium Gamete Formation. *Cell Reports*. **21**, 2017–2029 (2017).

829   111. Z. Bozdech *et al.*, The Transcriptome of the Intraerythrocytic Developmental Cycle of

830   Plasmodium falciparum. *PLoS Biol*. **1**, e5–16 (2003).

831   112. A. L. Vestergaard *et al.*, Critical roles of isoleucine-364 and adjacent residues in a

832   hydrophobic gate control of phospholipid transport by the mammalian P4-ATPase

833   ATP8A2. *Proc. Natl. Acad. Sci. U.S.A*. **111**, E1334–43 (2014).

834

Acknowledgements

Author Contributions

A.S.P., A.M., J.A.P., A.M.B., L.B., M.S., A.L.K., B.E., J.S.N.A, and M.H.L, carried out experiments; A.S.P., A.M., J.M.G., M.S., C.B.B., and M.H.L., analyzed the data; A.S.P., J.A.P., S.P.G., M.H.L., and M.T.D., designed experiments; A.S.P., M.H.L., and M.T.D., wrote the manuscript.

Competing Interests

The authors have no competing financial interests to declare.

Materials & Correspondence

Correspondence and requests for materials should be addressed to M.H.L. (mauld.lamarque@umontpellier.fr), or M.T.D. (mduraisi@hsph.harvard.edu).

Figure 1
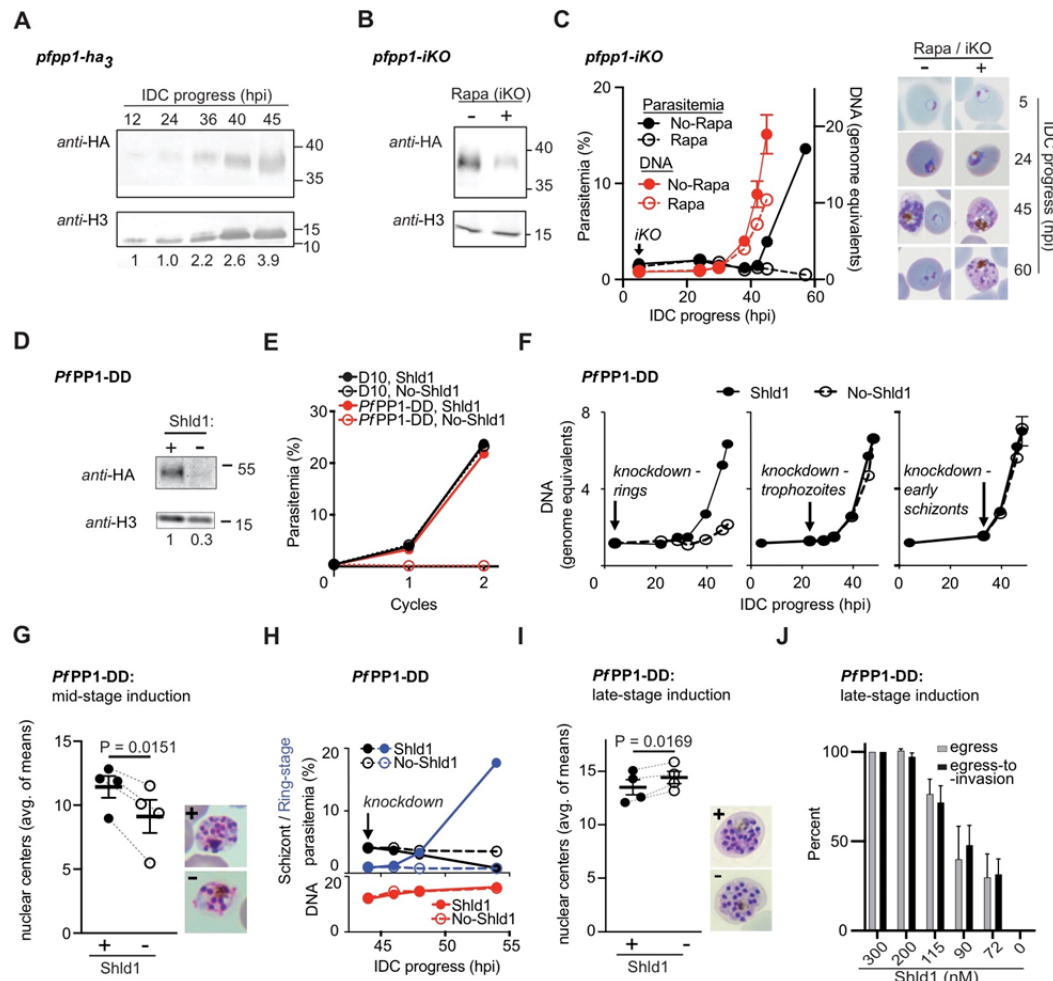
Fig. 1. Isolating an essential *Pf*PP1-function late in the intraerythrocytic developmental cycle. **(A)** *Pf*PP1-HA3 expression during intraerythrocytic development (hours post-invasion, hpi), assessed by immunoblot. Relative *Pf*PP1 levels (below lanes) are normalized to histone H3 loading controls. **(B)** iKO of *pfpp1* was initiated at 5 hpi with addition of rapamycin (Rapa) and protein levels were assessed by immunoblot at 30 hpi. **(C)** Left: Parasitemia and DNA synthesis over the IDC following +/-Rapa-treatment at 5 hpi in *pfpp1-iKO* parasites, monitored by flow-cytometry (mean +/- s.d.; n=3 technical replicates). Representative of 4 experiments. Right: Images of parasites along the IDC, following +/-Rapa-treatment at 5-hpi. **(D)** HA-tagged

865   *Pf*PP1-DD protein from schizont-stage parasites (~48 hpi) grown +/-Shld1 for 6 hrs, assessed by

866   immunoblot. **(E)** Proliferation of *Pf*PP1-DD and parental D10 parasites (wild type), +/-Shld1,

867   monitored by flow-cytometry. Knockdown was induced in cycle-zero. Representative of 2

868   experiments. **(F)** DNA replication in *Pf*PP1-DD parasites following knockdown (+/-Shld1) at the

869   indicated timepoints and stages of the IDC, monitored by flow-cytometry (mean +/- range; n=2

870   technical replicates; representative of 3 experiments for early ring induction, 2 experiments for

871   late-ring/trophozoite induction). **(G)** Left: Nuclear centers in terminally developed parasites,

872   assessed by light microscopy, with or without knockdown of *Pf*PP1-DD since the midpoint of

873   the IDC, 22-30 hpi (mean +/- s.e.m.; n=4 experiments). Right: Representative images of terminal

874   parasites +/-Shld1 (Giemsa-stained thin-blood smears). **(H)** Top: Schizont and ring-stage

875   parasites monitored by flow-cytometry following induction of *Pf*PP1-DD knockdown (+/-Shld1)

876   late in the IDC. Bottom: DNA content in the parallel samples, with addition of E64 (50 μM).

877   Representative of 2 biological replicates. **(I)** Nuclear centers following *Pf*PP1-DD knockdown at

878   44 hpi, as in (G). **(J)** Egress and egress-to-invasion following induction of partial *Pf*PP1-DD

879   knockdown at sublethal doses of Shld1. For this and all remaining panels, egress is based on the

880   rupture of schizonts, and egress-to-invasion is based on the number of ring-stage parasites

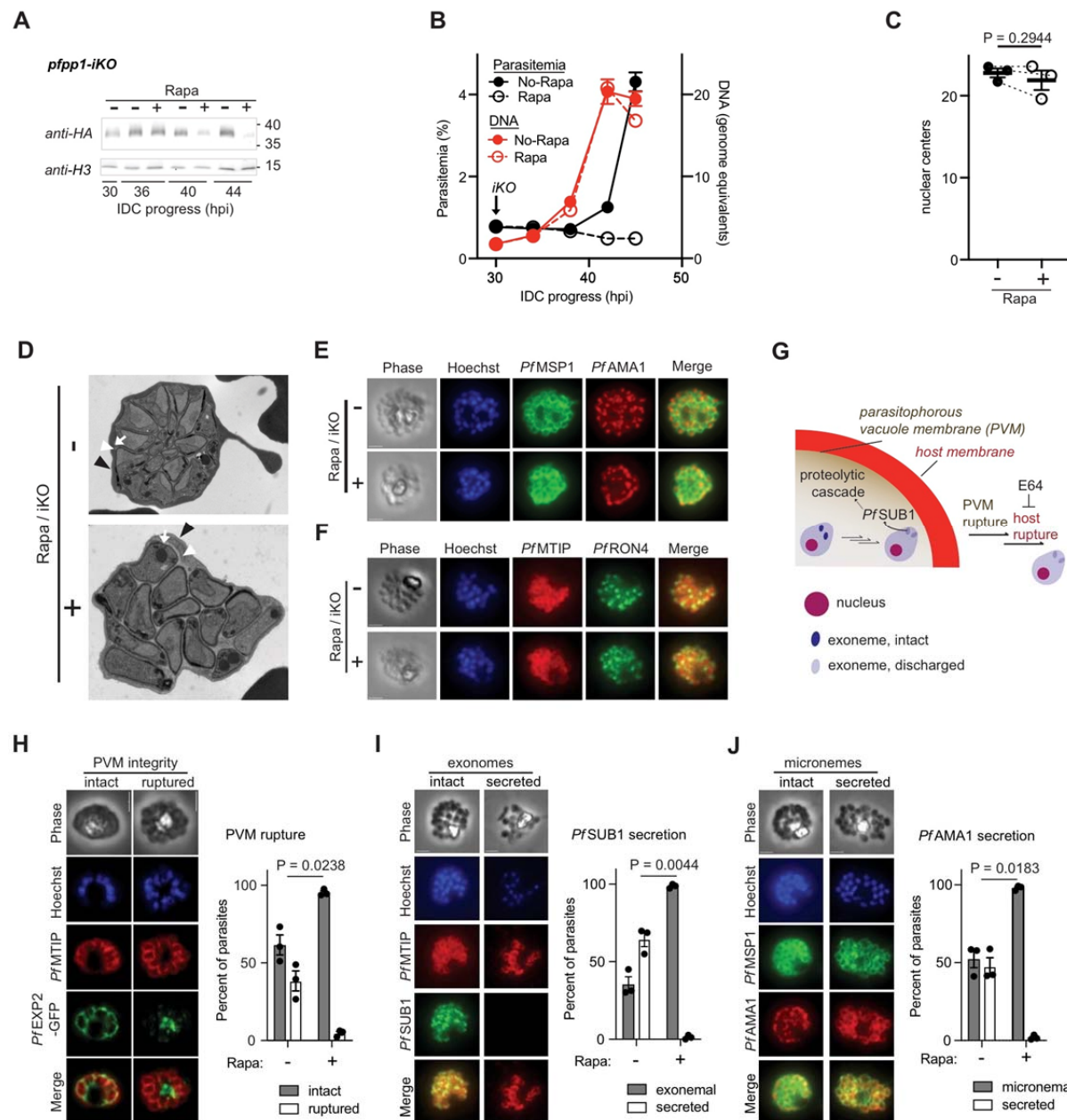881   following experimental treatment late in the IDC.

882

Figure 2

Fig. 2. *Pf*PP1 function an early step of parasite egress from erythrocytes. (**A**) *Pf*PP1-HA$_3$

expression +/- Rapa-mediated iKO of *pfpp1* at 30 hpi, assessed by immunoblot. (**B**) Parasitemia

and DNA synthesis following iKO of *pfpp1* at 30 hpi, as in Fig. 1C (mean +/- s.d.; n=3 technical

replicates). Representative of 4 experiments. (**C**) Nuclear centers in terminally developed

parasites following Rapa-mediated iKO of *pfpp1* at 30 hpi, as in Fig. 1 (mean +/- s.e.m.; n=3

889   experiments). **(D)** Electron microscopy of terminally developed *pfpp1*-iKO parasites treated +/-

890   Rapa at 30-hpi. In both images, the different membranes are indicated as follows: erythrocyte

891   (black   arrowhead),   PV   (white   arrowhead),   and   parasite   (white   arrow).   **(E-F)**

892   Immunofluorescence analysis of the microneme antigen *Pf*AMA1 (E) or the rhoptry-neck

893   antigen RON4 (F) in terminally developed parasites +/-iKO of *pfpp1* at 30 hpi. The images also

894   show the parasite plasma membrane marker MSP1 (E) and the inner membrane complex marker

895   MTIP (F). For both apical organelle markers, representative of 2 biological replicates. **(G)** In a

896   mature parasite, regulated secretion of *Pf*SUB1 from exonemes stimulates a proteolytic cascade

897   leading to sequential rupture of the PVM and the erythrocyte host membranes. **(H)** Assessment

898   of PVM rupture at 45 hpi in *pfpp1-iKO* / *Pf*EXP2-GFP parasites treated +/- Rapa at 30 hpi. Left:

899   immunofluorescence images of parasites with intact or ruptured PVMs. Right: Proportion of

900   infected cells exhibiting PVM rupture (mean +/- S.E.M.; n=3 experiments). Parasites in (H)-(J)

901   were treated with E64 (50 μM) at 41 hpi; the completion of cytokinesis was assessed with the

902   inner membrane complex marker *Pf*MTIP or the parasite plasma membrane marker *Pf*MSP1. **(I)**

903   With +/- Rapa-treatment at 30 hpi in *pfpp1*-iKO parasites, quantification of *Pf*SUB1 secretion

904   from exonemal compartments (loss of punctate fluorescence in images at left), as in (H) (mean

905   +/- S.E.M.; n=3 experiments). **(J)** Assessment of AMA1 secretion from micronemes, as in (H-I)

906   (mean +/- S.E.M.; n=3 experiments).
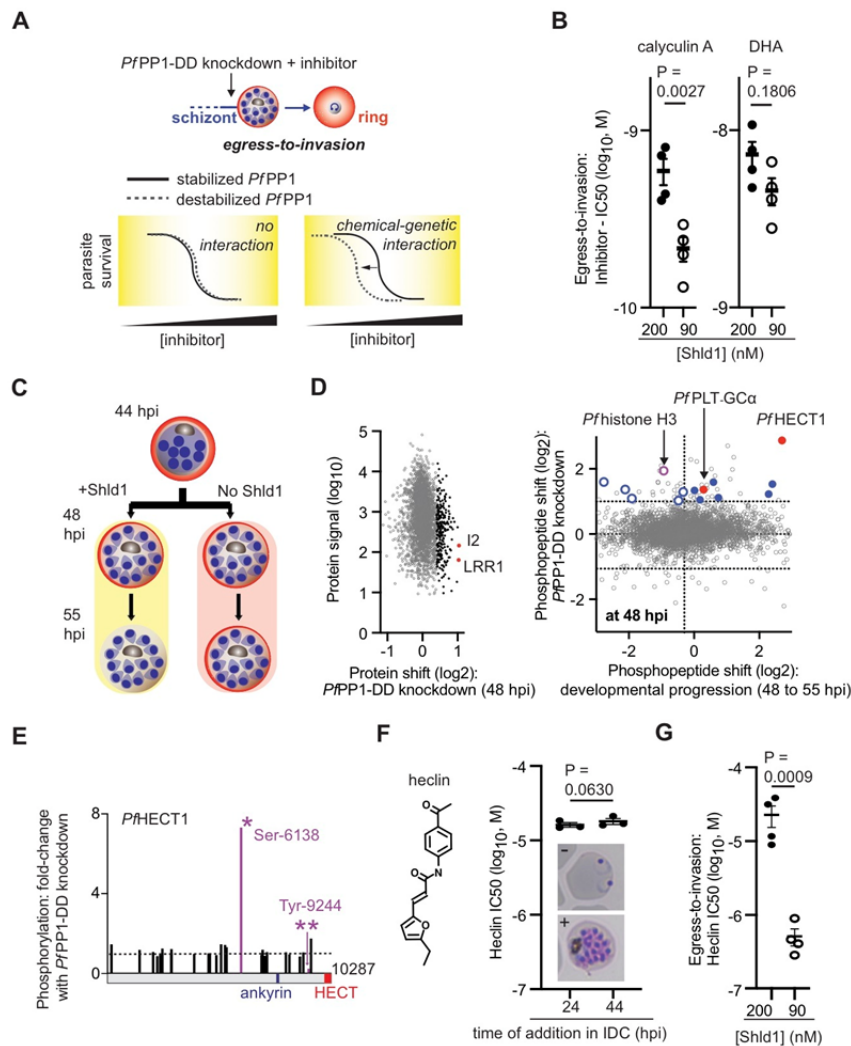
907

908

Figure 3

Fig. 3. *Pf*PP1 regulation of a HECT E3 protein ubiquitin-ligase for egress. (A) Chemical-genetics of *Pf*PP1-DD. We assessed the influence of inhibitors on *Pf*PP1-mediated egress-to-invasion (Fig. 1J) following administration to parasites late in the IDC. To test for functional interactions between *Pf*PP1 and processes targeted by inhibitor, we measured shifts in chemical sensitivity with partial destabilization of the DD-protein. **(B)** The sensitivity (IC50) of *Pf*PP1-mediated egress-to-invasion to the indicated inhibitors at 200 or 90 nM Shld1 (mean +/- s.e.m.; n=4 experiments). **(C)** Scheme for phosphoproteomic analysis of *Pf*PP1-DD knockdown late in the IDC, with samples obtained at 48- and 55-hpi. **(D)** Left: At 48 hpi, levels of individual

918   proteins (summed signal-to-noise) and shift in intensity with *Pf*PP1-knockdown. *Pf*Inhibitor 2

919   (I2) and *Pf*Leucine rich repeat (LRR) protein 1 are indicated in red, with the top 5% of

920   upregulated proteins indicated in black. Right: For all phosphopeptides detected in late-stage

921   parasites, a plot of changes in levels with *Pf*PP1-DD knockdown at 48-hpi (y-axis) versus

922   changes with development from 48 to 55-hpi in parasites on-Shld1 (x-axis). Two-fold increased

923   phosphorylation ($\log_2,1$) with knockdown is indicated. Up-phosphorylated phosphopeptides from

924   gene products increased in transcription at the schizont-stage (*30*) are colored; phosphopeptides

925   in the upper-right quadrant least likely to be affected by secondary, developmental-progression

926   defects (see Materials and Methods) are indicated with filled circles. Phosphorylation sites from

927   *Pf*histone H3, *Pf*HECT1, and *Pf*PLT-GCα, are marked in red. **(E)** Schematic of the *Pf*HECT1

928   protein encoded by PF3D7_0628100, with predicted domains. We show all phosphosites

929   detected in our study with magnitude of change with *Pf*PP1-DD knockdown at 48 hpi (Fig. 3D).

930   The most increased (Ser-6138) and decreased phosphorylation sites (Tyr-9244) are indicated

931   with symbols [*] and [**], respectively. **(F)** Sensitivity of *Pf*PP1-DD parasites on-Shld1 (0.5

932   µM) to heclin administered at the midpoint (24 hpi) or late in the IDC (44 hpi), determined from

933   erythrocyte re-invasion (mean +/- s.e.m.; n=3 experiments). Representative images of parasites at

934   55-hpi with or without heclin administration (100 µM) at 44 hpi, are shown below datapoints.

935   **(G)** The sensitivity of *Pf*PP1-mediated egress-to-invasion to heclin, as in (B) (mean +/- s.e.m.;
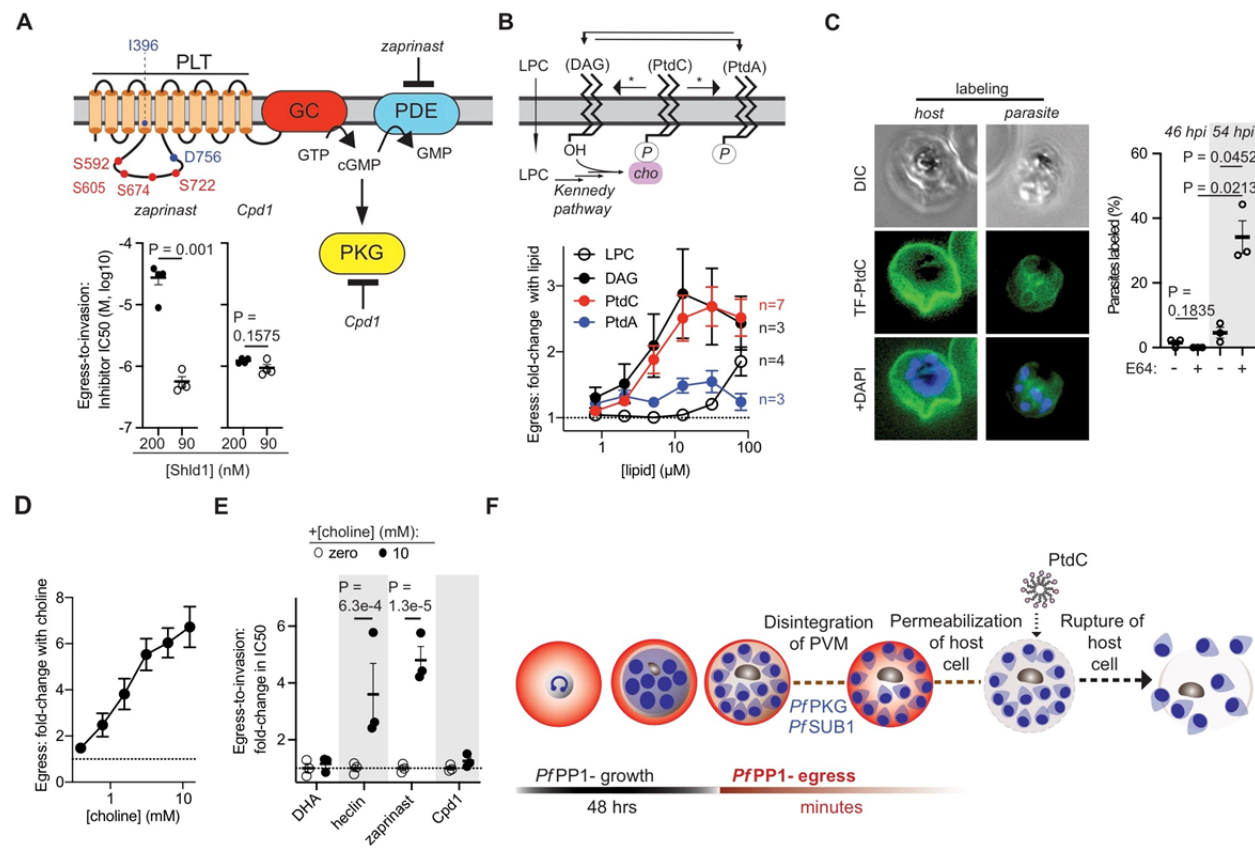
936   n=4 experiments).

937

Figure 4

Fig. 4: Regulation of egress by extracellular phosphatidylcholine. (**A**) Top: *Pf*PP1-regulated phosphorylation and cGMP-based signal transduction initiated by the parasite fusion protein carrying a phospholipid transporter (PLT) and a guanylyl cyclase (GC) domain (*Pf*PLT-GCα, PF3D7_1138400). We indicate *Pf*PP1-regulated sites in the PLT domain (red) and signature sequences for phospholipid translocase activity (purple), Ile-396 and Asp-756. cGMP-phosphodiesterase (PDE) and *Pf*PKG, as well as inhibitory small molecules for both targets, are depicted. Bottom: The sensitivity of *Pf*PP1-mediated egress-to-invasion to zaprinast (left) or Cpd1 (right), as in Fig. 3 (mean +/- s.e.m.; n=4 experiments). (**B**) Top: Phospholipids at the parasite plasma membrane. Interconversion of DAG and PtdA are likely mediated by parasite homologs of DAG-kinase and phosphatidic acid phosphatase (*73, 74*). Phospholipase enzymes

949   for conversion of PtdC to DAG and PtdC to PtdA (indicated with asterisks) have not been

950   identified in *Plasmodium falciparum* (*88*); PtdC levels are correlated with PtdA (*78*), indicating

951   linkage between the species. Extracellular LPC crosses the plasma membrane, providing

952   substrate for endogenous biosynthesis of PtdC via the Kennedy Pathway (*78, 79*). Bottom:

953   Stimulation of egress by exogenously administered lipids in parasites late in the IDC with partial

954   destabilization of *Pf*PP1-DD (100 nM Shld1), expressed in terms of fold-change relative to

955   egress without lipid (mean +/- s.e.m., with number of separate experiments indicated in plot). **(C)**

956   Labeling of the parasites by PtdC. Left: Representative images of late-stage, *P. falciparum*-

957   infected erythrocytes (*Pf*PP1-DD with 0.5 µM Shld1 and 50 µM E64, 54 hpi) labeled by TF-

958   PtdC at the erythrocyte membrane (host) or at the plasma membranes of internal parasites.

959   Nuclei are indicated by Hoechst dye. Right: The proportion of infected erythrocytes with labeled

960   parasites at the indicated timepoints, +/-E64 (mean +/- s.e.m.; n=3 experiments). **(D)** Stimulation

961   of *Pf*PP1-mediated egress with supplementation of choline, as in (B). **(E)** Modulation of *Pf*PP1-

962   regulated cellular processes by supplemented choline. For each inhibitor, fold-change in IC50

963   with additional choline in *Pf*PP1-DD parasites in 150 nM Shld1 is indicated (mean +/- s.e.m.;

964   n=3 experiments; multiple *t*-tests). **(F)** A model for the function of *Pf*PP1 through the IDC.

965   Following activity in growth during the IDC, *Pf*PP1 is essential for the egress program upstream

966   of *Pf*PKG and the *Pf*SUB1-initiated proteolytic cascade required for disintegration of the PVM.

967   PtdC enters host cells following natural permeabilization of the erythrocyte membrane, acting on

968   exposed parasites to stimulate egress.

969

Supplementary Information for

Co-option of *Plasmodium falciparum* PP1 for egress from host erythrocytes

Aditya S. Paul[1], Alexandra Miliu[2], Joao A. Paulo[3], Jonathan M. Goldberg[1], Arianna M. Bonilla[1], Laurence Berry[2], Marie Séveno[2], Catherine Braun-Breton[2], Aziz L. Kosber[1], Brendan Elsworth[1], Jose S.N. Arriola[1], Maryse Lebrun[2], Steven P. Gygi[3], Mauld H. Lamarque[2], Manoj T. Duraisingh[1]

This file includes:

> Supplementary Text
> Figs. S1 to S6
> Tables S1 to S5

Supplementary Text

Assessment of the specificity of PfPP1-function according to phosphoproteomic data. At 48-hpi,

30 phosphopeptides (0.8% of 3884 total detected) exhibit a reduction of >2-fold with *Pf*PP1-DD

destabilization, and 60 (1.5% of total) are increased by >2-fold (Table S3). Other evidence

suggests limited effects secondary to perturbation of *Pf*PP1-function at 48-hpi: (i) proliferation

defects elicited by knockdown are reversible to a large degree with resupplementation of Shld1

at 48-hpi, but not 55-hpi (Fig. S4A); (ii) in contrast to 55-hpi, changes in the global

phosphoproteome with *Pf*PP1-DD knockdown at 48-hpi are not predictive of further

developmental progression (Fig. 3D; fig. S4B); and (iii) overall variability in the phosphopeptide

levels at 48-hpi, but not 55-hpi, induced by *Pf*PP1-DD-destabilization is comparable to a

baseline, determined from the distribution of non-phosphorylated peptides in the same sample

(Fig. S4C) (*110*). Of the phosphopeptides upregulated by >2-fold with *Pf*PP1-DD knockdown at

48-hpi (y-axis, Fig. 3D), we regarded sites that did not decrease with IDC progression from 48 to

55-hpi (x-axis, Fig. 3D) to be least likely to be influenced by effects secondary to perturbation of
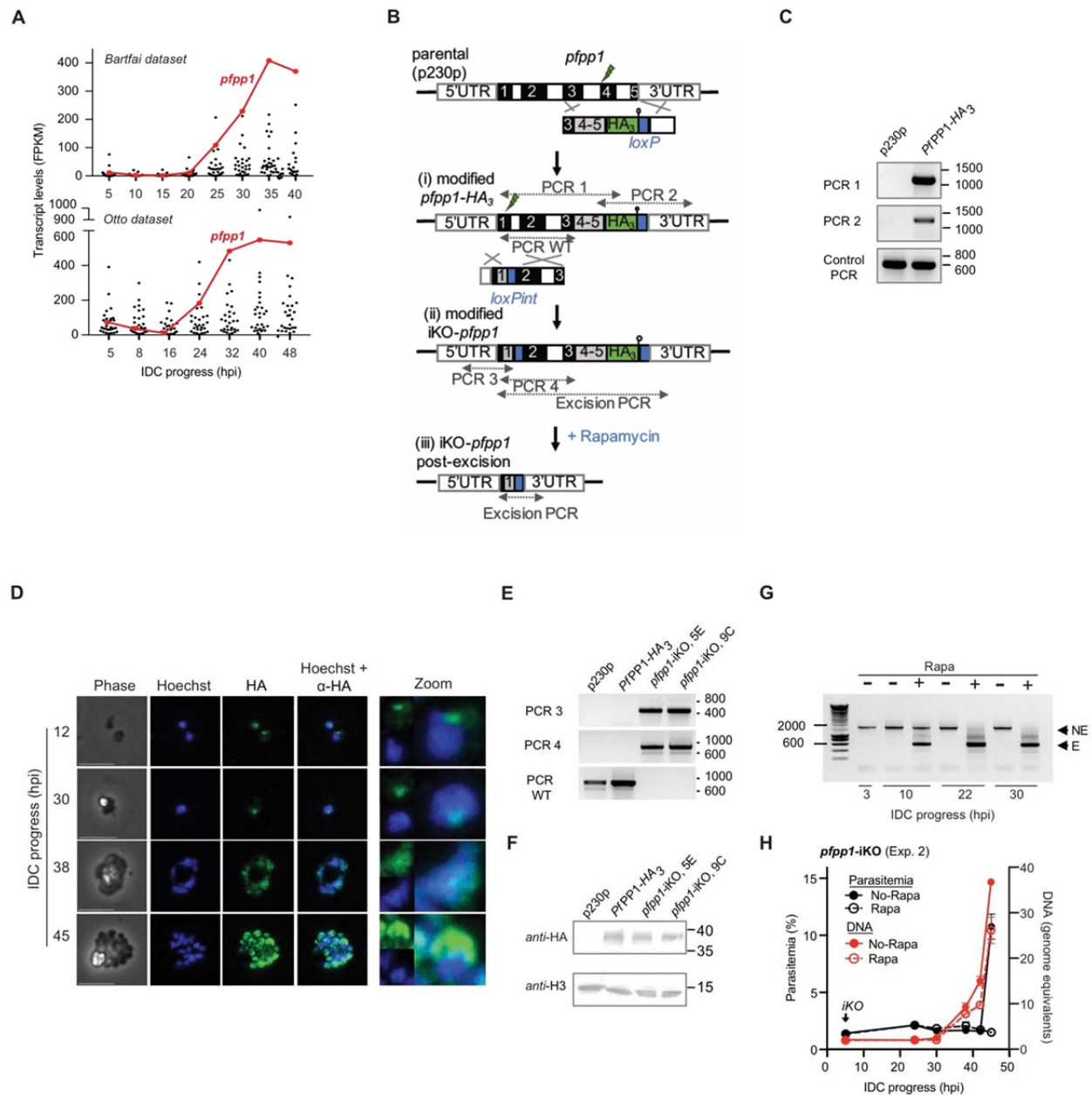
*Pf*PP1.

Figure S1

1008

1009   **Figure S1. (A)** For 29 *P. falciparum* protein phosphatase genes (*8*), levels of mRNA expression (frequency per

1010   kilobase per millions reads, fpkm) over the course of the IDC measured in two separate transcriptome-wide studies

1011   from Bártfai and colleagues (top), and Otto and colleagues (bottom) (*29, 30*). **(B)** Sequential double-crossover

1012   recombination at the *pfpp1* chromosomal locus in the DiCre recombinase-expressing p230p parental parasite line to

1013   generate (i) the *Pf*PP1-HA₃ line with a 3' loxP site; and (ii) the *pfpp1*-iKO with a loxP-containing synthetic intron

1014   (loxPint); followed by (iii) treatment with rapamycin to induce excision of *pfpp1*. Sites for PCR amplicons to

1015 confirm construction of transgenic lines are indicated. Black and white bars represent exons and introns of the *pfpp1*

1016 gene, respectively. Grey bars represent recodonized region of the *pfpp1* gene and blue bars stand for loxP site.

1017 Lollipop: stop codon; green lightning bolt: Cas9 double strand break. **(C)** PCRs to confirm construction of *Pf*PP1-

1018 HA$_3$ with 3'-loxP, as in (B). **(D)** Localization of *Pf*PP1-HA$_3$, relative to Hoechst-stained nuclei, assessed by

1019 immunofluorescence**.** Staging is indicated by IDC progress. **(E)** PCRs to confirm construction of *pfpp1*-iKO with

1020 loxP-containing synthetic intron, as in (B). PCR also confirm unmodified *pfpp1* (PCR WT). **(F)** Immunoblot

1021 performed with anti-HA antibodies to show that *Pf*PP1-HA$_3$-loxP and *pfpp1*-iKO parasite lines express a tagged

1022 version of the protein of the same molecular mass. Anti-histone H3 was used as a loading control. **(G)** PCRs to

1023 confirm Rapa-induced excision of the *pfpp1* gene in *pfpp1*-iKO transgenic line following rapamycin treatment at 3

1024 hpi. NE and E indicate the non excised (1606 bp) and excised (581 bp) versions of *pfpp1* gene, respectively. Sizes

1025 are indicated on the left in bp. **(H)** A second experiment to measure the effect on DNA replication and proliferation

1026 in *pfpp1-iKO* parasites following +/- Rapa-treatment at 5 hpi, as in Fig. 1C.
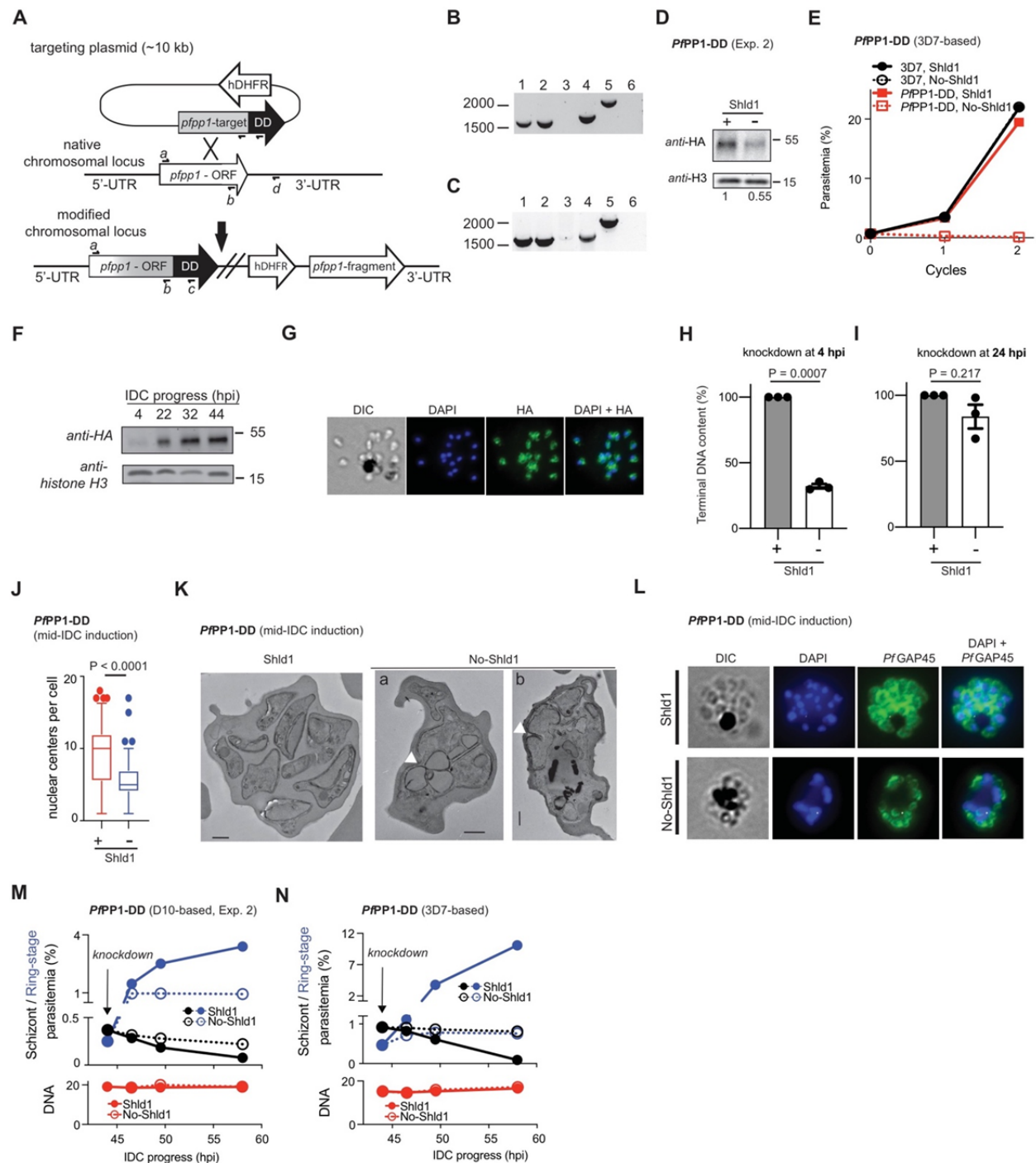
1027

Figure S2

Figure S2. (A) Top: Scheme for single-crossover integration of the *dd-tag* into the endogenous *pfpp1* genetic locus, with binding sites for diagnostic primers indicated. **(B-C)** PCR to confirm integration of *dd* into *pfpp1* in the D10 (B) and 3D7 background strains (C). In electrophoresis gel, lanes 1,3,5: wild type parasite background; lanes 2,4,6:

53

1033   clonal *Pf*PP1-DD transgenic parasites. Lanes 1,2: diagnostic primers *a,b*; lanes 3,4: primers *a,c*; lanes 5,6: primers

1034   *a,d*. Positions by size (bp) are indicated. **(D)** An immunoblot as in Fig. 1D, schizont-stage *Pf*PP1-DD parasites

1035   grown +/-0.2 μM Shld1 for ~20 hrs. **(E)** Proliferation of *Pf*PP1-DD in the 3D7 background, assessed as in Fig. 1E.

1036   **(F)** *Pf*PP1-DD expression in synchronized parasites in 0.2 μM Shld1 at the indicated timepoints following

1037   erythrocyte invasion, assessed with anti-HA tag antibody. Histone H3 levels were measured for loading control. **(G)**

1038   Assessment of *Pf*PP1 localization in a recently ruptured *Pf*PP1-DD schizont-stage parasite using an antibody for

1039   HA. Nuclear staining was carried out with DAPI. **(H-I)** DNA content in advanced-stage parasites (51-55 hpi) +/-

1040   induction of *Pf*PP1-DD knockdown early (4 hpi, H) or at a mid-stage of the IDC (24 hpi, I), assessed by flow-

1041   cytometry. **(J)** Box plot of numbers of nuclear centers (median, outliers at >95% percentile with none observed

1042   below 5%) in terminally developed parasites with induction of *Pf*PP1-DD knockdown at a mid-stage of the IDC

1043   (experiment from Fig. 1F, middle panel). Two-tailed Mann-Whitney test. **(K)** Electron microscopy images of

1044   terminally developed *Pf*PP1-DD parasites (55 hpi), with knockdown induced at 24 hpi (+/-0.3 μM Shld1). Parasites

1045   were supplemented with 50 μM E64 at ~47 hpi to block egress. For knockdown-cells (No-Shld1), we show parasites

1046   arrested at a late stage when incipient cytokinesis in the vicinity of dividing nuclei are apparent (white arrowheads).

1047   **(L)** Immunofluorescence microscopy images of terminally developed *Pf*PP1-DD parasite cells, with knockdown and

1048   sampling as in (K), indicating the inner membrane complex marker *Pf*GAP45. **(M-N)** Egress and erythrocyte re-

1049   invasion following knockdown of *Pf*PP1-DD in either the D10 (M) or the 3D7 background (N) at 44 hpi, and DNA

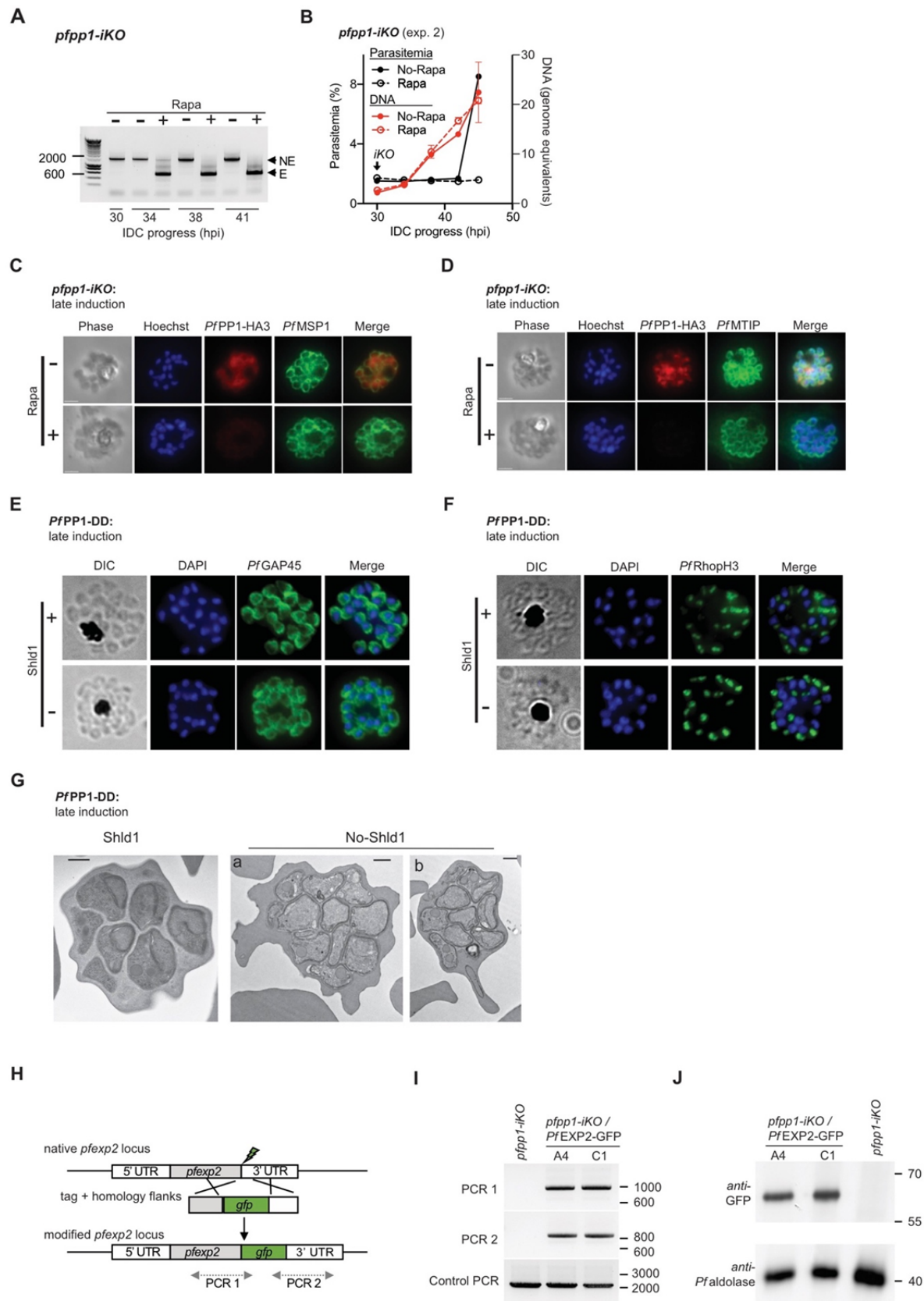1050   content in E64-treated parasites (50 μM) as described in Fig. 1H.

1051

Figure S3

1053   **Figure S3. (A)** PCR to confirm excision of the *pfpp1* gene following iKO with rapamycin at 30hpi (trophozoite

1054   stage), as in fig. S1G. **(B)** A second experiment measuring parasitemia and DNA synthesis following iKO of *pfpp1*,

1055   as in Fig. 2B. **(C-D)** Immunofluorescence images showing depletion of *Pf*PP1-HA$_3$ in parasites assessed in Figs. 2E

1056   (C) and 2F (D). **(E-F)** Immunofluorescence microscopy images of *Pf*PP1-DD parasite cells, sampled at 55 hpi,

1057   indicating the inner membrane complex marker *Pf*GAP45 (E) or the rhoptry marker *Pf*RhopH3 (F), with knockdown

1058   (+/- 0.5 µM Shld1) induced at 44 hpi. Parasites were supplemented with 50 µM E64 to block egress. **(G)** Electron

1059   microscopy images of terminally developed *Pf*PP1-DD parasites treated as in (E-F). **(H)** Modification of the native

1060   *pfexp2* locus for 3'-tagging with GFP in the *pfpp1*-iKO background, via Cas9-mediated double-stranded break repair

1061   (see fig. S1B). **(I)** PCRs to confirm construction of *pfpp1*-iKO / *Pf*EXP2-GFP, as in (H). **(J)** Immunoblot to show

1062   GFP expression in *pfpp1-iKO / Pf*EXP2-GFP lines. *Pf*aldoase was assessed to control for loading.
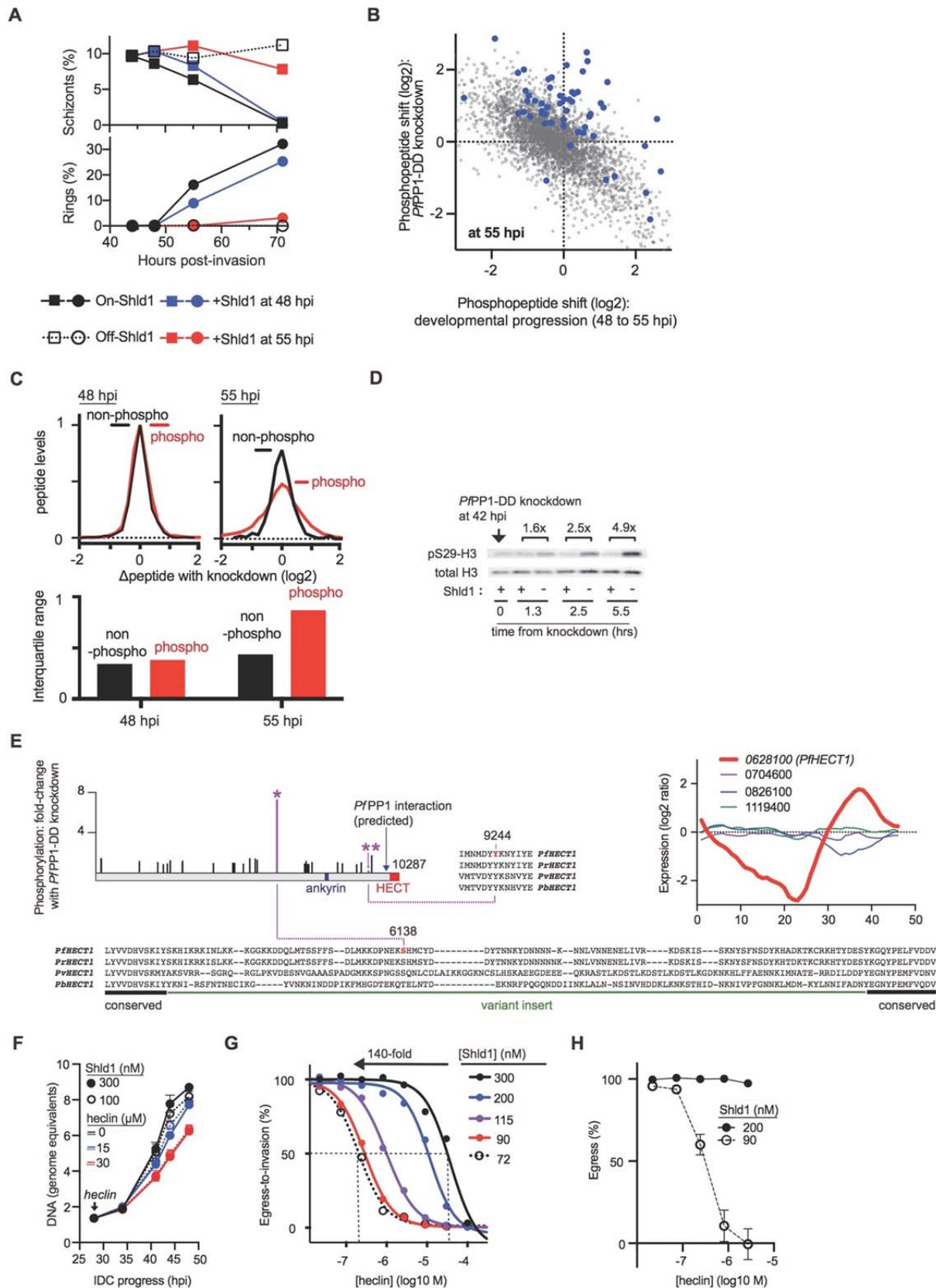
1063

Figure S4

Figure S4. (A) Timecourse of schizont and ring-stage parasitemia in control samples for phosphoproteomic analysis of *Pf*PP1-DD knockdown, assessed from thin blood smears. Parasites were maintained continuously on-Shld1 (0.3 µM) or off-Shld1 (EtOH) following start of experiment at 44 hpi. To assess reversibility of the knockdown-phenotype, off-Shld1 parasites were supplemented with Shld1 (1 µM) at the two timepoints for sample collection. **(B)** The effect of *Pf*PP1-DD-based perturbation on levels of all detected phosphopeptides at 55-hpi plotted against changes with development (+Shld1-parasites) from 48 to 55-hpi, as in Fig. 3D. All phosphopeptides upregulated by >2-fold at 48-hpi by *Pf*PP1-DD knockdown (Fig. 3D) are indicated in blue, showing that these hits are masked by developmental effects dominant by 55-hpi. **(C)** Top: Following TiO2-based affinity purification, the distribution of the log2-fold differences with *Pf*PP1-DD knockdown for either the enriched phosphopeptides (red) or non-phosphorylated peptides (black) measured by mass-spectrometry. Data for samples collected at both the 48 (left) and 55-hpi timepoints (right) are shown. Bottom: The interquartile ranges for data shown in top panel. **(D)** Phospho-histone H3 (Ser-29) dynamics with *Pf*PP1-knockdown in parasites late in the IDC, assessed by immunoblot analysis. The timepoint of *Pf*PP1-knockdown and timepoints for sampling following knockdown are indicated. The fold-increase in phospho-histone H3 (S29), normalized to total histone H3, is indicated above the blot (mean of 2 technical replicate timecourses). **(E)** Left: Schematic of *Pf*HECT1 as in Fig. 3E with *Pf*PP1-regulated phosphosites shown in sequence alignment with orthologs from other *Plasmodium* spp. (*P. reichenowi*, *Pr*; *P. vivax*, *Pv*; *P. berghei*, *Pb*). For Ser-6138, extended sequence is shown to highlight regions of conservation and variation. Position of the predicted interaction site for *Pf*PP1 (*34*) is shown (blue arrow). Right: Relative transcript expression over the course of IDC (*111*) for the 4 HECT domain-containing proteins in *P. falciparum*, each denoted by the 7-digit suffix of the systematic gene ID beginning with "PF3D7_". **(F)** DNA replication in *Pf*PP1-DD parasites following administration of heclin at 28-hpi with indicated concentrations (DMSO control, black, 15 µM, blue; 30 µM, red;), and growth supported by a high (300 nM) or suboptimal (100 nM) concentration of Shld1 (mean +/- s.e.m.; n=3 experiments). **(G)** Dose-response curves from a single experiment to measure susceptibility of egress-to-invasion by *Pf*PP1-DD parasites to heclin at various Shld1 concentrations, with range of IC50 values indicated. **(H)** The susceptibility of egress by *Pf*PP1-DD parasites to heclin at 200 or 90 nM Shld1 (mean +/- s.e.m.; n=3 experiments).
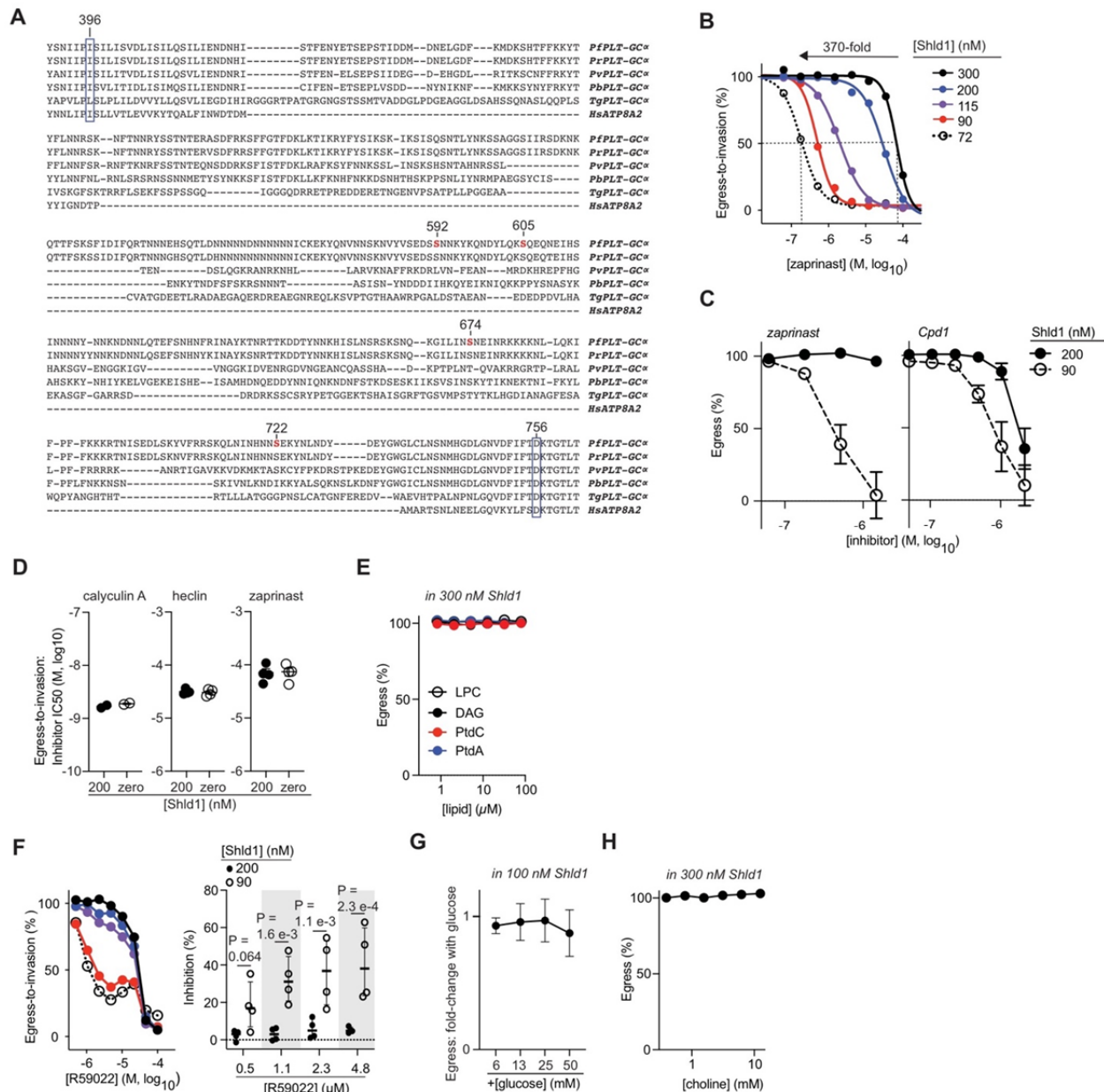
Figure S5

Figure S5. (A) Alignment of the multi-phosphorylated cytoplasmic domain between the fourth and fifth transmembrane domains of the PLT in *Pf*PLT-GCα (see Fig. 4A). The alignment shows orthologs from *P. reichenowi* (*Pr*), *P. vivax* (*Pv*), *P. berghei* (*Pb*), and *T. gondii* (*Tg*); and also the human protein ATP8A2 (UniProt Q9NTI2.2) to show conservation of a isoleucine residue (396 in *Pf*PLT-GCα) in transmembrane 4 required for transport of phospholipids (*112*), indicated in purple. *Pf*PP1-responsive phosphorylation sites are indicated in red. The absolutely conserved catalytic aspartate residue in the consensus

1098   sequence DKTGTLT required for ATPase-dependent phospholipid transport is indicated in purple. **(B)** An

1099   experiment with dose-responses of *Pf*PP1-DD parasites to zaprinast (egress-to-invasion) elicited over a multiple

1100   Shld1 concentrations, with range of IC50 values indicated. **(C)** Sensitivity of egress by *Pf*PP1-DD parasites to

1101   zaprinast (left) or Cpd1 (right). **(D)** The sensitivity of egress-to-invasion by D10 parasites (parent to *Pf*PP1-DD) for

1102   the indicated compounds at the indicated Shld1 concentrations (mean +/- s.e.m.; n=2-4 experiments as indicated).

1103   **(E)** In 300 nM Shld1, percent egress for *Pf*PP1-DD parasites in the presence of the lipids in Fig. 4B at the indicated

1104   concentrations (mean +/- s.e.m.; n=4 experiments). **(F)** Left: A series of dose-response curves in a single experiment

1105   showing induced sensitivity of parasite egress-to-invasion to R59022 with knockdown of *Pf*PP1-DD at

1106   concentrations <10 µM. Shld1 concentrations as in (B). Right: Induced sensitivity of parasites to low concentrations

1107   (<10 µM) of R59022 with partial knockdown of *Pf*PP1-DD, based on inhibition of egress-to-invasion (mean +/-

1108   s.e.m.; n=4 experiments). Significance assessed by multiple *t*-tests. **(G)** In 100 nM Shld1, the effect of

1109   supplementation with the indicated concentrations of glucose on egress by *Pf*PP1-DD parasites, expressed as fold-

1110   change compared to no-added glucose (mean +/- s.e.m.; n=4 experiments). The baseline concentration of glucose in

1111   media is 11.1 mM. **(H)** In 300 nM Shld1, percent egress for choline (see Fig. 4E) at indicated concentrations, as in

1112   (E) (mean +/- s.e.m.; n=4 experiments).
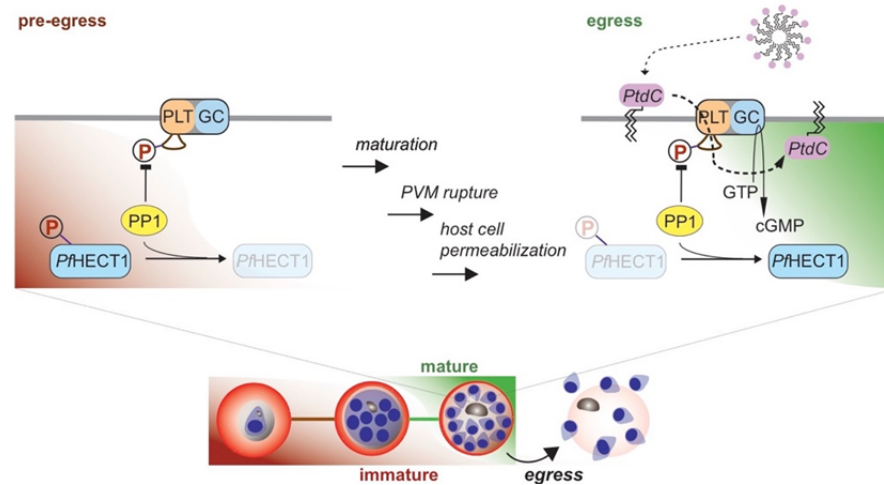
1113

Figure S6

Figure S6. *Pf*PP1-regulated cellular pathways in coordination with late IDC-stage developmental progression of *P. falciparum*. At an immature state when the parasite is not yet competent to process signals for egress (pre-egress), *Pf*PP1 acts on *Pf*PLT-GCα to suppress cGMP levels. *Pf*PP1 acts on *Pf*HECT1 as the parasite matures, and cGMP activates the egress program leading to PVM rupture and host cell permeabilization. We propose that PtdC from the serum is translocated by *Pf*PLT-GCα, providing a late signal to stimulate egress.

1121   **Table S1.** Proteomic analysis of *Pf*PP1-DD parasites in late IDC-stage parasites.

1122   **Table S2.** A second proteomic analysis of *Pf*PP1-DD parasites in late IDC-stage parasites.

1123   **Table S3.** Phosphoproteomic analysis of *Pf*PP1-DD parasites in late IDC-stage parasites.

1124   **Table S4.** Gene Ontology analysis of proteins upregulated with *Pf*PP1-DD knockdown in late IDC-stage parasites.

1125   **Table S5.** Primers used in this study.